MULTISCALE MODEL. SIMUL.
Vol. 21, No. 1, pp. 80–118

SPECKLE MEMORY EFFECT IN THE FREQUENCY DOMAIN AND STABILITY IN TIME-REVERSAL EXPERIMENTS*

JOSSELIN GARNIER† AND KNUT SØLNA‡

Abstract. When waves propagate through a complex medium like the turbulent atmosphere the wave field becomes incoherent and the wave intensity forms a complex speckle pattern. In this paper we study a speckle memory effect in the frequency domain and some of its consequences. This effect means that certain properties of the speckle pattern produced by wave transmission through a randomly scattering medium is preserved when shifting the frequency of the illumination. The speckle memory effect is characterized via a detailed novel analysis of the fourth-order moment of the random paraxial Green's function at four different frequencies. We arrive at a precise characterization of the frequency memory effect and what governs the strength of the memory. As an application we quantify the statistical stability of time-reversal wave refocusing through a randomly scattering medium in the paraxial or beam regime. Time reversal refers to the situation when a transmitted wave field is recorded on a time-reversal mirror then time reversed and sent back into the complex medium. The re-emitted wave field then refocuses at the original source point. We compute the mean of the refocused wave and identify a novel quantitative description of its variance in terms of the radius of the time-reversal mirror, the size of its elements, the source bandwidth, and the statistics of the random medium fluctuations.

Key words. waves in random media, multiple scattering, time reversal, parabolic approximation, broadband beam, memory effect

MSC codes. 60H15, 35R60, 35L05

DOI. 10.1137/22M1470414

1. Introduction.

For imaging or communication purposes it is important to understand how waves propagate through a randomly scattering medium. The quantities of interest can generally be expressed in terms of statistical averages. Usually the first- and second-order moments of the Green's function are sufficient to characterize them. However in some circumstances fourth-order moments are needed, for instance, for scintillation problems [10, 14] or the analysis of intensity correlation-based imaging [2, 22]. For imaging with narrow or broad band signals it is also important to characterize multifrequency moments [4]. We consider here the paraxial regime corresponding to high-frequency and long-range propagation of a wave beam. The paraxial regime is physically relevant and it models many situations, for instance, laser beam propagation [1, 30] or underwater acoustics [31]. The equations that govern the evolution of the fourth-order moments in the paraxial regime have been known for a long time [32] and [20, sect. 20.18]. The solution of the fourth-order moment problem was recently analyzed and discussed in [14, 15] when the four Green's functions involved

* Received by the editors January 10, 2022; accepted for publication (in revised form) August 11, 2022; published electronically February 2, 2023.
https://doi.org/10.1137/22M1470414

Funding: The first author was supported by the Agence Nationale pour la Recherche under Grant ANR-19-CE46-0007 (project ICCI) and Air Force Office of Scientific Research under grant FA9550-22-1-0176. The second author was supported by the Air Force Office of Scientific Research under grant FA9550-22-1-0176 and the National Science Foundation under grant DMS-2010046.

† CMAP, CNRS, Ecole Polytechnique, Institut Polytechnique de Paris, 91128 Palaiseau Cedex, France (josselin.garnier@polytechnique.edu).

‡ Department of Mathematics, University of California, Irvine, CA 92697 USA (ksolna@math.uci.edu).

in the fourth-order moment are evaluated at the same frequency. In this paper, we extend this result to the case when the four Green's functions have different frequencies. This new result makes it possible to analyze a number of configurations in wave propagation and imaging. Here we consider two main motivating applications.

The first motivating application is time-harmonic wave focusing through a random medium. Wavefront-shaping–based schemes [27, 29, 33, 34, 35] have attracted attention in recent years, particularly because of their potential applications for focusing and imaging through scattering media. The primary goal is to focus monochromatic light through a layer of strongly scattering material. This is a challenging problem as multiple scattering of waves scrambles the transmitted light into random interference intensity patterns called speckle patterns [19]. This is shown in Figure 1.1(a): without control of the source the intensity of the transmitted field forms a complex speckle pattern. However, by using a spatial light modulator (SLM) before the scattering medium, it is possible to focus light as first demonstrated in [34]. Indeed, the elements of the SLM can impose phase shifts, and an optimization scheme makes it possible to choose the phase shifts so as to maximize the intensity transmitted at one target point behind the scattering medium. This is shown in Figure 1.1(b). The optimal phase shifts depend on the medium, and they are equal to the opposite phases of the field emitted by a point source at the target point and recorded in the plane of the SLM [25]. In other words, the wavefront-shaping optimization procedure is equivalent to phase conjugation or time reversal. This is illustrated in Figure 1.2 which describes a time-reversal experiment. A time-reversal experiment consists of two steps, and it is based on the use of a special device, a time-reversal mirror (TRM), that is used as an array of receivers in the first step and as an array of sources in the second step. The first step is described in Figure 1.2(a): a point source emits a wave that propagates through a scattering medium and that is recorded by the TRM. The second step is described in Figure 1.2(b): the recorded signals are time-reversed and re-emitted into the same medium by the TRM, and the re-emitted waves then focus at the original source point. At a single frequency this process corresponds to phase conjugation or re-emission of the complex conjugate of the recorded wave field by the TRM; with some abuse of notation we refer to this process as time-harmonic time reversal. It has been shown that the speckle memory effect [7, 11] allows to focus on a neighboring point close to the original target point [33, 34, 35], which opens the way for the transmission of spatial patterns [16, 17, 18, 28]. Indeed, one the main manifestations of the spatial memory effect is the following one: by applying an appropriate and deterministic spatial phase modulation to the conjugated source field in the second step of the time-reversal experiment (Figure 1.2(b)) one can achieve that the focusing (red spot) in the bottom right plot is shifted. By properly composing such modulated source fields one can transmit a pattern; see [16] for a detailed discussion. A main question we want to address here is whether such speckle memory effects can be exploited also in the frequency domain. In fact, we show that it is possible to focus a time-harmonic signal with a different frequency than the one of the field recorded by the TRM in Figure 1.2(a). One can even focus a broadband pulse and this opens the way to the transmission of short pulses; see [25] for experimental verification of the frequency memory effect. The process then corresponds to using and processing the reference phase-conjugated field in Figure 1.2(b) in order to focus coherently time-harmonic waves with slightly shifted frequencies. The reference field or a "guide star" field may then be used over a frequency band to obtain focusing for pulses. The theoretical description of such a frequency memory effect has so far been an open question. In section 6 we give a quantitative description of the effect of a

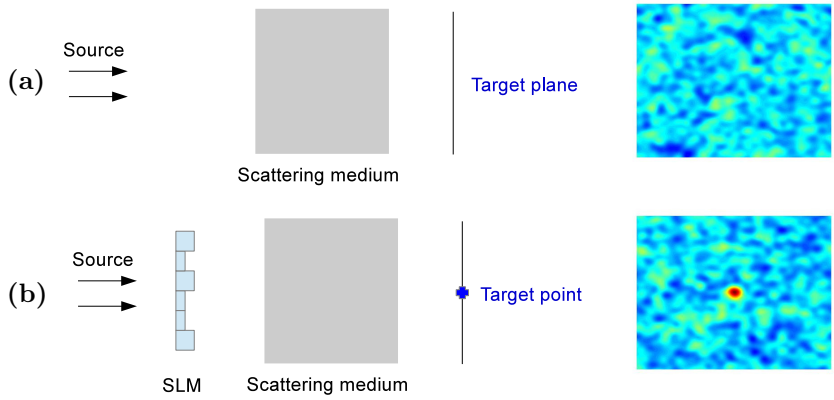

FIG. 1.1. *Focusing wave through a scattering medium. Without any control one gets a speckle pattern in the target plane* (a). *With an SLM one can focus on a target point by imposing appropriate phase shifts* (b) *(From* [16]*).*

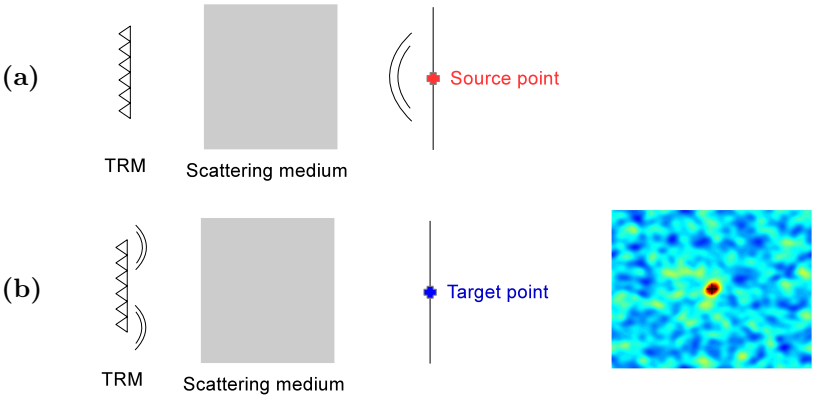

FIG. 1.2. *Time-reversal experiment through a scattering medium. In the first step of the experiment* (a) *a time-harmonic point source emits a wave that propagates through the scattering medium and is recorded by the TRM used as an array of receivers. In the second step of the experiment* (b) *the TRM is used as an array of sources; it emits the complex-conjugated recorded field, and the wave refocuses at the original source location (the cross in the right image stands for the original source location; the focal spot is centered at the cross) (From* [16]*).*

frequency shift on refocusing, which is directly related to the speckle memory effect in the frequency domain. We show that the speckle pattern is only slightly changed when shifting the frequency so that we can use the same source phase field over a range of frequencies and still obtain focusing for all frequencies in the band. A main result presented in section 6 is that the width Ω of the frequency band for which we can use the same recorded and conjugated field at the TRM and still achieve focusing is determined by the speckle coherence frequency $\Omega_{\rm spec}$:

$$\Omega \lesssim \Omega_{\rm spec} := \frac{\ell_{\rm par}}{LT}, \tag{1.1}$$

where $T = L/c_o$ is the travel time over the distance L from the source to the TRM for a background wave speed c_o and $\ell_{\rm par}$ is the paraxial distance introduced in (5.32) below. The paraxial distance corresponds to the travel distance at which the paraxial

description of the wave beam in the random medium breaks down and is inversely proportional to a measure of the lateral scattering strength in the random medium. It follows that for longer propagation distances and stronger medium fluctuations the frequency band at which the frequency memory holds becomes narrower since the speckle pattern then becomes more sensitive to a shift in the source frequency.

The second motivation for our multifrequency analysis is statistical stability in time reversal. Time reversal for waves in random media has indeed been studied theoretically, numerically, and experimentally (see the review [8]). As mentioned above when a wave is emitted by a point source and recorded by a TRM, which then re-emits the time-reversed recorded signals, then in general the wave refocuses on the original source location; see Figure 1.2. It moreover turns out that refocusing is enhanced when the medium is randomly scattering, and that the time-reversed refocused wave is statistically stable, in the sense that its shape depends on the statistical properties of the random medium, but not on its particular realization. The phenomenon of focusing enhancement has been analyzed quantitatively [3, 9, 24, 26]. Statistical stability of time-reversal refocusing for broadband pulses is usually qualitatively proved by invoking the fact that the time-reversed refocused wave is the superposition of many independent frequency components, which gives the self-averaging property in the time domain [3, 26]. However, so far, there has not been a fully satisfactory analysis of the statistical stability phenomenon, because it involves the evaluation of a fourth-order moment of the Green's function of the random wave equation. This problem has been addressed in [21] in a situation similar to the one addressed in this paper, but using the circular complex Gaussian assumption for the evaluation of the fourth-order moments that are needed for the analysis. Here we will not make use of this assumption, rather we will prove that the fourth-order moments can be computed, and this allows us to give a detailed analysis of the statistical stability of the time-reversed refocused wave. In section 7 we quantify time-reversal refocusing and stability as functions of the size of the TRM, the size of its elements, the source bandwidth, and the statistical properties of the random medium. The main results can be summarized as follows: if the bandwidth B of the source is small so that $B \ll \Omega_{\rm spec}$ and also if the scattering is strong enough so that the spreading of the beam is large relative to its original width, then the signal-to-noise ratio (SNR) of the refocused wave is roughly equal to the number of elements in the TRM:

$$\text{SNR} \simeq N \text{ for } N := \left(\frac{r_0}{\rho_0}\right)^2, \tag{1.2}$$

with r_0 being the size of the TRM and ρ_0 the size of the elements. If the bandwidth B of the source is large so that $B \gg \Omega_{\rm spec}$ and if scattering is strong, then

$$\text{SNR} \simeq \left(\frac{N}{8}\right)\left(\frac{B}{\Omega_{\rm spec}}\right). \tag{1.3}$$

This shows that the source bandwidth improves the statistical stability of the refocused wave, provided it is larger than the speckle coherence frequency. This then quantifies the usual assertion found in the literature that the profile of the time-reversed field is self-averaging by independence of the frequency components of the wave field and clarifies the hypotheses which ensure that such a result is valid. We remark here also that in the strongly scattering situation and small mirror elements it is a classic result that the time-reversal refocusing resolution R can be expressed as the Rayleigh resolution formula $R \approx \lambda L/A_{\rm eff}$ evaluated at the central wavelength λ

and at the scattering-enhanced aperture $A_{\rm eff}$ which scales with propagation distance as $L^{3/2}$ [16]. In the notation introduced here this means that

$$R \approx \lambda \sqrt{\frac{\ell_{\rm par}}{L}}, \tag{1.4}$$

where we need $\ell_{\rm par} > L$ for the paraxial approximation to be valid. Note that this resolution measure is independent of the actual TRM radius.

The paper is organized as follows. First in section 2 we outline the main setting with scalar waves propagating in a random medium and summarize the main result regarding the paraxial approximation that we use, the solution of the Itô–Schrödinger equation. In section 3 we describe the two main applications that we have introduced: time-harmonic refocusing and broadband time reversal. In sections 4–5 we study in detail the second- and fourth-order moments of the paraxial Green's function at different frequencies and how we get successively simpler expressions for the moments by making further assumptions regarding the scaling regime. We quantify the focusing properties of the two main applications in terms of resolution and stability in sections 6–7. In Appendix A we discuss in more detail the scaling regime that we use and how it relates to the Itô–Schrödinger equation that is fundamental to our asymptotic moment analysis.

2. Paraxial waves in random media. We consider scalar waves and assume the governing equation

$$(\partial_z^2 + \Delta_{\boldsymbol{x}})u - \frac{n^2(z,\boldsymbol{x})}{c_o^2}\partial_t^2 u = 0, \tag{2.1}$$

for $(z,\boldsymbol{x}) \in \mathbb{R}\times\mathbb{R}^2$, the space coordinates. In (2.1) $n(z,\boldsymbol{x})$ is the local index of refraction that we model as random. We remark that even though the scalar wave equation is simple and linear, the relation between the statistics of the index of refraction and the statistics of the wave field is highly nontrivial and nonlinear. Originally motivated by elastic problems in geophysics, we assume that the privileged propagation axis is the z-direction and will consider beam waves propagating into the z-direction, thus corresponding to the horizontal direction in Figures 1.1 and 1.2. We model moreover the complex medium as a random medium and do this by letting the local index of refraction in (2.1) be parameterized by

$$n^2(z,\boldsymbol{x}) = 1 + \nu(z,\boldsymbol{x}) \tag{2.2}$$

for ν being the centered random medium fluctuations. We assume that ν is a stationary zero-mean random field that is mixing in z and with integrable correlations.

It is now convenient to Fourier transform in time:

$$\hat{u}(\omega,z,\boldsymbol{x}) = \int_{\mathbb{R}} u(t,z,\boldsymbol{x}) \exp\big(i\omega t\big) dt. \tag{2.3}$$

We then obtain the Helmholtz or reduced wave equation:

$$(\partial_z^2 + \Delta_{\boldsymbol{x}})\hat{u} + \frac{\omega^2}{c_o^2} n^2(z,\boldsymbol{x})\hat{u} = 0, \tag{2.4}$$

with $k = \omega/c_o$ being the free space wavenumber.

A particular solution of (2.4) in the case of a homogeneous medium $n \equiv 1$ is a plane wave propagating in the z direction:

$$\hat{u} = \exp\Big(i\frac{\omega}{c_o}z\Big).$$

We make the ansatz of a slowly varying envelope around a plane wave going into the z-direction

$$\hat{u}(\omega, z, \boldsymbol{x}) = \exp\Big(i\frac{\omega}{c_o}z\Big)v(\omega, z, \boldsymbol{x}). \tag{2.5}$$

In the white-noise paraxial regime (which holds when the wavelength is much smaller than the correlation length of the medium and the beam radius, which are themselves much smaller than the propagation distance) we can then model v in terms of the solution of the following Itô–Schrödinger equation:

$$2ikdv + \Delta_{\boldsymbol{x}} v\, dz + k^2 v \circ dB(z, \boldsymbol{x}) = 0. \tag{2.6}$$

In Appendix A we discuss in detail the scaling assumptions of the white-noise paraxial regime leading to the model (2.6). We remark that the symbol $\circ$ stands for the Stratonovich stochastic integral, $B(z, \boldsymbol{x})$ is a real-valued Brownian field over $[0, \infty) \times \mathbb{R}^2$ with covariance

$$\mathbb{E}[B(z, \boldsymbol{x})B(z', \boldsymbol{x}')] = \min\{z, z'\}C(\boldsymbol{x} - \boldsymbol{x}'), \tag{2.7}$$

and C is determined by the two-point statistics of the fluctuations of the random medium as

$$C(\boldsymbol{x}) = \int_{\mathbb{R}} \mathbb{E}[\nu(0, \mathbf{0})\nu(z, \boldsymbol{x})]dz, \tag{2.8}$$

with ν being the random medium fluctuations in (2.2). Note that the width of C is the correlation length of the medium fluctuations. The Itô–Schrödinger equation was analyzed for the first time in [5], and it was derived from first principles by a multiscale analysis of the wave equation in a random medium in [13]. The model (2.6) leads to closed equations for wave field moments of all orders. We discuss in the appendix the first-order moment equation that is readily solvable. The second-order one-frequency moment equations are also explicitly solvable, while the fourth-order equations are not explicitly solvable in the white-noise paraxial regime, neither in the one-frequency nor in the multifrequency cases. However, in a secondary scaling regime that we denote the scintillation regime we will be able to solve both the second-order and fourth-order multifrequency moments. We will push through this moment analysis in section 5. Before this, in section 3, we discuss the detailed modeling of the two applications which motivates the particular form of the second- and fourth-order multifrequency moments that we consider. In section 4 we express these moments in terms of the moments of the Green's function associated with the Itô–Schrödinger equation (2.6).

3. Time-reversal experiment. We assume that a TRM is located in the plane $z = 0$. The radius of the mirror is R_{m} and the radius of its elements is ρ_0.

3.1. Time-harmonic refocusing experiment. In the first step of the time-harmonic time-reversal experiment, a point source localized at $(\boldsymbol{y}, L)$ emits a time-harmonic signal at frequency $\tilde{\omega}$ (see Figure 3.1). The TRM is used as an array of receivers and records the wave emitted by the point source. The size ρ_0 of the elements of the TRM is taken into account in the form of a Gaussian smoothing kernel with radius ρ_0. We denote the time-harmonic Green's function from $(\boldsymbol{x}_m, 0)$ to $(\boldsymbol{y}, L)$ by $\hat{\mathcal{G}}(\tilde{\omega}, L, \boldsymbol{y}, \boldsymbol{x}_m)$ (which is equal to the Green's function from $(\boldsymbol{y}, L)$ to $(\boldsymbol{x}_m, 0)$

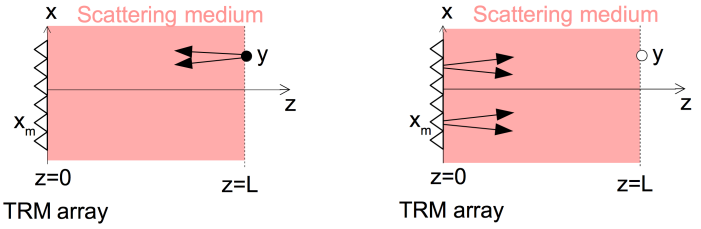

FIG. 3.1. *Time-reversal experiment. Left: first step of the experiment (a point source transmits from* $(\boldsymbol{y}, L)$ *and the TRM in the plane* $z = 0$ *is used as an array of receivers). Right: second step of the experiment (the TRM is used as an array of sources).*

by reciprocity). By last term in the next equation (3.1) we remove the expected phase $\tilde{\omega}L/c_o$ from the time-harmonic field at frequency $\tilde{\omega}$ recorded at $(\boldsymbol{x}_m, 0)$ and get

$$\hat{u}_{\rm rec}(\boldsymbol{x}_m;\boldsymbol{y}) = \frac{1}{2\pi\rho_0^2}\int_{\mathbb{R}^2}\hat{\mathcal{G}}(\tilde{\omega}, L, \boldsymbol{y}, \boldsymbol{x}_m+\boldsymbol{x}')\exp\Big(-\frac{|\boldsymbol{x}'|^2}{2\rho_0^2}\Big)d\boldsymbol{x}'\exp\Big(-i\frac{\tilde{\omega}}{c_o}L\Big). \tag{3.1}$$

In the second step of the experiment, the TRM is used as an array of sources. It emits the complex-conjugated (time-reversed) recorded field $\overline{\hat{u}_{\rm rec}}$ at frequency ω, which can be different from $\tilde{\omega}$. From the field observed in the plane $z = L$ at the point $(\boldsymbol{x}, L)$ we again remove the expected phase $\omega L/c_o$ and get

$$\hat{u}_{\rm tr}(\boldsymbol{x};\boldsymbol{y}) = \int_{\mathbb{R}^2}\hat{u}_{\rm em}(\omega,\boldsymbol{x};\boldsymbol{x}_m)\exp\Big(-\frac{|\boldsymbol{x}_m|^2}{R_{\rm m}^2}\Big)\overline{\hat{u}_{\rm rec}(\boldsymbol{x}_m;\boldsymbol{y})}d\boldsymbol{x}_m\exp\Big(-i\frac{\omega}{c_o}L\Big). \tag{3.2}$$

Here we have assumed that the TRM has a radius $R_{\rm m}$ and can be modeled by a Gaussian spatial cut-off function. Moreover, we again take into account the size ρ_0 of the elements of the TRM by considering that from any point $(\boldsymbol{x}_m, 0)$ the TRM can transmit from an element with radius ρ_0 and with a Gaussian form, which generates the following field at point $(\boldsymbol{x}, L)$:

$$\hat{u}_{\rm em}(\omega,\boldsymbol{x};\boldsymbol{x}_m) = \frac{1}{2\pi\rho_0^2}\int_{\mathbb{R}^2}\hat{\mathcal{G}}(\omega, L, \boldsymbol{x}, \boldsymbol{x}_m+\boldsymbol{x}')\exp\Big(-\frac{|\boldsymbol{x}'|^2}{2\rho_0^2}\Big)d\boldsymbol{x}'. \tag{3.3}$$

The time-reversed field observed in the plane $z = L$ can therefore be expressed as

$$\begin{aligned}\hat{u}_{\rm tr}(\boldsymbol{x};\boldsymbol{y}) = {}& \frac{4\omega\tilde{\omega}K_0}{c_o^2}\exp\Big(i\frac{\tilde{\omega}-\omega}{c_o}L\Big)\iint_{\mathbb{R}^2\times\mathbb{R}^2}\exp\Big(-\frac{|\boldsymbol{x}'|^2}{r_0^2}-\frac{|\boldsymbol{y}'|^2}{4\rho_0^2}\Big)\\ &\times\hat{\mathcal{G}}\big(\omega, L, \boldsymbol{x}, \boldsymbol{x}'+\frac{\boldsymbol{y}'}{2}\big)\overline{\hat{\mathcal{G}}\big(\tilde{\omega}, L, \boldsymbol{y}, \boldsymbol{x}'-\frac{\boldsymbol{y}'}{2}\big)}d\boldsymbol{x}'d\boldsymbol{y}',\end{aligned} \tag{3.4}$$

with

$$K_0 = \frac{c_o^2(r_0^2-\rho_0^2)}{16\pi\omega\tilde{\omega}\rho_0^2r_0^2}, \qquad r_0^2 = R_{\rm m}^2+\rho_0^2. \tag{3.5}$$

From now on we will take $K_0 = 1$ as this multiplicative factor does not play any role in what follows.

The goal of the forthcoming analysis is to quantity the refocusing properties in terms of resolution and stability and to make it precise for which frequency offset $\omega - \tilde{\omega}$ it is possible to observe refocusing.

Remark. In this paper we model the global shape of the TRM and the local shape of the elements of the TRM by soft Gaussian cut-off functions, instead of hard cut-off functions such as $\mathbf{1}_{[0,R_{\rm m}]}(|\boldsymbol{x}_m|)$ or $\mathbf{1}_{[0,\rho_0]}(|\boldsymbol{x}'|)$, because this makes it possible to get simpler expressions. This does not affect qualitatively the results.

3.2. Broadband time-reversal experiment. In the first step of the broadband time-reversal experiment, a point source localized at $(\boldsymbol{y}, L)$ emits a short pulse $f(t)$ (see Figure 3.1). The pulse has central frequency ω_0 and bandwidth B. The TRM in the plane $z = 0$ is used as an array of receivers and records the wave emitted by the point source around the expected arrival time L/c_o:

$$u_{\rm rec}\big(t, \boldsymbol{x}_m; \boldsymbol{y}\big) = \frac{1}{(2\pi)^2\rho_0^2}\int_{\mathbb{R}}\int_{\mathbb{R}^2} \hat{\mathcal{G}}(\omega, L, \boldsymbol{y}, \boldsymbol{x}_m + \boldsymbol{x}') \times \exp\Big(-\frac{|\boldsymbol{x}'|^2}{2\rho_0^2} - i\omega\Big(\frac{L}{c_o} + t\Big)\Big)\hat{f}(\omega)d\boldsymbol{x}'d\omega. \tag{3.6}$$

In the second step of the experiment, the TRM is used as an array of sources. It emits the time-reversed recorded field. We observe the field around the original source location $(\boldsymbol{y}, L)$ and around the expected arrival time L/c_o to study the wave refocusing:

$$u_{\rm tr}(t, \boldsymbol{x}; \boldsymbol{y}) = \frac{1}{2\pi}\int_{\mathbb{R}}\int_{\mathbb{R}^2} \hat{u}_{\rm em}(\omega, \boldsymbol{x}; \boldsymbol{x}_m)\exp\Big(-\frac{|\boldsymbol{x}_m|^2}{R_{\rm m}^2}\Big)\overline{\hat{u}_{\rm rec}(\omega, \boldsymbol{x}_m; \boldsymbol{y})} \times \exp\Big(-i\omega\Big(\frac{L}{c_o} + t\Big)\Big)d\boldsymbol{x}_m d\omega, \tag{3.7}$$

with $\hat{u}_{\rm em}(\omega, \boldsymbol{x}; \boldsymbol{x}_m)$ defined by (3.3) and $\hat{u}_{\rm rec}(\omega, \boldsymbol{x}_m; \boldsymbol{y})$ being the Fourier transform of $u_{\rm rec}(t, \boldsymbol{x}_m; \boldsymbol{y})$ given by (3.6). We aim at characterizing the statistical stability of the refocused wave, in terms of the number of elements of the TRM and in terms of bandwidth of the pulse, as well as the refocusing resolution.

We consider the case when the bandwidth B of f is smaller than its central frequency ω_0, for instance, when the source is a modulated Gaussian with central frequency ω_0 and bandwidth B:

$$\hat{f}(\omega) = \frac{\sqrt{2\pi}}{B}\exp\Big(-\frac{(\omega-\omega_0)^2}{2B^2}\Big). \tag{3.8}$$

The time-reversed field observed in the plane $z = L$ around the expected arrival time L/c_o can be expressed as

$$u_{\rm tr}(t, \boldsymbol{x}; \boldsymbol{y}) = \frac{4\omega_0^2}{2\pi c_o^2}K_0\int_{\mathbb{R}}\iint_{\mathbb{R}^2\times\mathbb{R}^2} \exp\Big(-\frac{|\boldsymbol{x}'|^2}{r_0^2} - \frac{|\boldsymbol{y}'|^2}{4\rho_0^2} - i\omega t\Big)\overline{\hat{f}(\omega)} \times \hat{\mathcal{G}}\Big(\omega, L, \boldsymbol{x}, \boldsymbol{x}' + \frac{\boldsymbol{y}'}{2}\Big)\overline{\hat{\mathcal{G}}\Big(\omega, L, \boldsymbol{y}, \boldsymbol{x}' - \frac{\boldsymbol{y}'}{2}\Big)}d\boldsymbol{x}'d\boldsymbol{y}'d\omega, \tag{3.9}$$

with $K_0 = [c_o^2(r_0^2 - \rho_0^2)]/[16\pi\omega_0^2\rho_0^2r_0^2]$. Corresponding to the situation above we will take $K_0 = 1$ below.

The goal of the forthcoming analysis is to quantity the refocusing properties in terms of resolution and stability and to clarify the role of the source bandwidth as well as the parameters of the TRM.

4. The Green's function in the white-noise paraxial regime. In the white-noise paraxial regime the Green's function $\hat{\mathcal{G}}$ is of the form [15]

$$\hat{\mathcal{G}}(\omega, L, \boldsymbol{x}, \boldsymbol{y}) = \frac{ic_o}{2\omega}e^{i\frac{\omega}{c_o}L}\hat{G}(\omega, L, \boldsymbol{x}, \boldsymbol{y}),$$

where ω/c_o is the homogeneous wavenumber and the function $\hat{G}$ is the solution of the Itô–Schrödinger equation introduced in (2.6):

$$d\hat{G}(\omega,z,\boldsymbol{x},\boldsymbol{y}) = \frac{ic_o}{2\omega}\Delta_{\boldsymbol{x}}\hat{G}(\omega,z,\boldsymbol{x},\boldsymbol{y})dz + \frac{i\omega}{2c_o}\hat{G}(\omega,z,\boldsymbol{x},\boldsymbol{y})\circ dB(z,\boldsymbol{x}), \tag{4.1}$$

with the initial condition in the plane $z=0$: $\hat{G}(\omega,z=0,\boldsymbol{x},\boldsymbol{y}) = \delta(\boldsymbol{x}-\boldsymbol{y})$.

In this context, the time-reversed field (3.4) observed at $(\boldsymbol{x},L)$ when the original source is at $(\boldsymbol{y},L)$ in the wave refocusing experiment of section 3.1 is

$$\begin{aligned}\hat{u}_{\rm tr}(\boldsymbol{x};\boldsymbol{y}) = \iint_{\mathbb{R}^2\times\mathbb{R}^2} &\exp\Big(-\frac{|\boldsymbol{x}'|^2}{r_0^2} - \frac{|\boldsymbol{y}'|^2}{4\rho_0^2}\Big)\\ &\times \hat{G}\big(\omega,L,\boldsymbol{x},\boldsymbol{x}'+\frac{\boldsymbol{y}'}{2}\big)\overline{\hat{G}\big(\tilde{\omega},L,\boldsymbol{y},\boldsymbol{x}'-\frac{\boldsymbol{y}'}{2}\big)}d\boldsymbol{x}'d\boldsymbol{y}'.\end{aligned} \tag{4.2}$$

The mean time-reversed field is

$$\mathcal{M}_1(\boldsymbol{x};\boldsymbol{y}) = \mathbb{E}\big[\hat{u}_{\rm tr}(\boldsymbol{x};\boldsymbol{y})\big], \tag{4.3}$$

and it can be expressed as

$$\begin{aligned}\mathcal{M}_1(\boldsymbol{x};\boldsymbol{y}) = \iint_{\mathbb{R}^2\times\mathbb{R}^2} &\exp\Big(-\frac{|\boldsymbol{x}'|^2}{r_0^2} - \frac{|\boldsymbol{y}'|^2}{4\rho_0^2}\Big)\\ &\times \mathbb{E}\Big[\hat{G}\big(\omega,L,\boldsymbol{x},\boldsymbol{x}'+\frac{\boldsymbol{y}'}{2}\big)\overline{\hat{G}\big(\tilde{\omega},L,\boldsymbol{y},\boldsymbol{x}'-\frac{\boldsymbol{y}'}{2}\big)}\Big]d\boldsymbol{x}'d\boldsymbol{y}'.\end{aligned}$$

The covariance function of the time-reversed field is

$$\mathcal{M}_2(\boldsymbol{x},\tilde{\boldsymbol{x}};\boldsymbol{y}) = \mathbb{E}\big[\hat{u}_{\rm tr}(\boldsymbol{x};\boldsymbol{y})\overline{\hat{u}_{\rm tr}(\tilde{\boldsymbol{x}};\boldsymbol{y})}\big], \tag{4.4}$$

and it can be expressed as

$$\begin{aligned}\mathcal{M}_2(\boldsymbol{x},\tilde{\boldsymbol{x}};\boldsymbol{y}) = \iint_{\mathbb{R}^2\times\mathbb{R}^2} &\exp\Big(-\frac{|\boldsymbol{x}_1{}'|^2+|\boldsymbol{x}_2{}'|^2}{r_0^2} - \frac{|\boldsymbol{y}_1{}'|^2+|\boldsymbol{y}_2{}'|^2}{4\rho_0^2}\Big)\\ &\times \mathbb{E}\Big[\hat{G}\big(\omega,L,\boldsymbol{x},\boldsymbol{x}_1{}'+\frac{\boldsymbol{y}_1{}'}{2}\big)\hat{G}\big(\tilde{\omega},L,\boldsymbol{y},\boldsymbol{x}_2{}'+\frac{\boldsymbol{y}_2{}'}{2}\big)\\ &\times\overline{\hat{G}\big(\tilde{\omega},L,\boldsymbol{y},\boldsymbol{x}_1{}'-\frac{\boldsymbol{y}_1{}'}{2}\big)\hat{G}\big(\omega,L,\tilde{\boldsymbol{x}},\boldsymbol{x}_2{}'-\frac{\boldsymbol{y}_2{}'}{2}\big)}\Big]d\boldsymbol{x}_1{}'d\boldsymbol{y}_1{}'d\boldsymbol{x}_2{}'d\boldsymbol{y}_2{}'.\end{aligned}$$

These expressions show that we need to study the second- and fourth-order moments of the random paraxial Green's functions at different frequencies.

5. The moments of the Green's function. This section contains the detailed analysis of the second- and fourth-order moments that are needed to study the time-reversed field.

5.1. The second-order moment. Let us consider two frequencies $\omega,\tilde{\omega}$. We consider the second-order moment:

$$\begin{aligned}M_1(z,\boldsymbol{x},\boldsymbol{y}) = \iint_{\mathbb{R}^2\times\mathbb{R}^2} &\exp\Big(-\frac{|\boldsymbol{x}'|^2}{r_0^2} - \frac{|\boldsymbol{y}'|^2}{4\rho_0^2}\Big)\\ &\times \mathbb{E}\Big[\hat{G}\big(\omega,z,\boldsymbol{x},\boldsymbol{x}'+\frac{\boldsymbol{y}'}{2}\big)\overline{\hat{G}\big(\tilde{\omega},z,\boldsymbol{y},\boldsymbol{x}'-\frac{\boldsymbol{y}'}{2}\big)}\Big]d\boldsymbol{x}'d\boldsymbol{y}'.\end{aligned} \tag{5.1}$$

M_1 satisfies the system:

$$\frac{\partial M_1}{\partial z} = \frac{ic_o}{2}\left(\frac{1}{\omega}\Delta_{\boldsymbol{x}} - \frac{1}{\tilde{\omega}}\Delta_{\boldsymbol{y}}\right) M_1 + \frac{1}{8c_o^2}\big(2\omega\tilde{\omega}C(\boldsymbol{x}-\boldsymbol{y}) - (\omega^2+\tilde{\omega}^2)C(\mathbf{0})\big)M_1, \tag{5.2}$$

starting from

$$M_1(z=0,\boldsymbol{x},\boldsymbol{y}) = \exp\Big(-\frac{|\boldsymbol{x}+\boldsymbol{y}|^2}{4r_0^2} - \frac{|\boldsymbol{x}-\boldsymbol{y}|^2}{4\rho_0^2}\Big).$$

5.2. The fourth-order moment. Let us consider four frequencies $\omega_1, \omega_2, \tilde{\omega}_1$, $\tilde{\omega}_2$. We consider the fourth-order moment

$$\begin{aligned} &M_2(z,\boldsymbol{x}_1,\boldsymbol{x}_2,\boldsymbol{y}_1,\boldsymbol{y}_2) \\ &= \iint_{\mathbb{R}^2\times\mathbb{R}^2\times\mathbb{R}^2\times\mathbb{R}^2} \exp\Big(-\frac{|\boldsymbol{x}_1'|^2+|\boldsymbol{x}_2'|^2}{r_0^2} - \frac{|\boldsymbol{y}_1'|^2+|\boldsymbol{y}_2'|^2}{4\rho_0^2}\Big) \\ &\quad\times \mathbb{E}\Big[\hat{G}\big(\omega_1,z,\boldsymbol{x}_1,\boldsymbol{x}_1'+\frac{\boldsymbol{y}_1'}{2}\big)\hat{G}\big(\omega_2,z,\boldsymbol{x}_2,\boldsymbol{x}_2'+\frac{\boldsymbol{y}_2'}{2}\big) \\ &\quad\times \hat{G}\big(\tilde{\omega}_1,z,\boldsymbol{y}_1,\boldsymbol{x}_1'-\frac{\boldsymbol{y}_1'}{2}\big)\hat{G}\big(\tilde{\omega}_2,z,\boldsymbol{y}_2,\boldsymbol{x}_2'-\frac{\boldsymbol{y}_2'}{2}\big)\Big] d\boldsymbol{x}_1' d\boldsymbol{y}_1' d\boldsymbol{x}_2' d\boldsymbol{y}_2'. \end{aligned} \tag{5.3}$$

It satisfies

$$\begin{aligned} \frac{\partial M_2}{\partial z} &= \frac{ic_o}{2}\Big(\frac{1}{\omega_1}\Delta_{\boldsymbol{x}_1} + \frac{1}{\omega_2}\Delta_{\boldsymbol{x}_2} - \frac{1}{\tilde{\omega}_1}\Delta_{\boldsymbol{y}_1} - \frac{1}{\tilde{\omega}_2}\Delta_{\boldsymbol{y}_2}\Big)M_2 \\ &\quad + \frac{1}{4c_o^2}U_2\big(\boldsymbol{x}_1,\boldsymbol{x}_2,\boldsymbol{y}_1,\boldsymbol{y}_2\big)M_2, \end{aligned} \tag{5.4}$$

with the generalized potential

$$\begin{aligned} U_2\big(\boldsymbol{x}_1,\boldsymbol{x}_2,\boldsymbol{y}_1,\boldsymbol{y}_2\big) &= \omega_1\tilde{\omega}_1 C(\boldsymbol{x}_1-\boldsymbol{y}_1) + \omega_1\tilde{\omega}_2 C(\boldsymbol{x}_1-\boldsymbol{y}_2) + \omega_2\tilde{\omega}_1 C(\boldsymbol{x}_2-\boldsymbol{y}_1) \\ &\quad + \omega_2\tilde{\omega}_2 C(\boldsymbol{x}_2-\boldsymbol{y}_2) - \omega_1\omega_2 C(\boldsymbol{x}_1-\boldsymbol{x}_2) - \tilde{\omega}_1\tilde{\omega}_2 C(\boldsymbol{y}_1-\boldsymbol{y}_2) \\ &\quad - \frac{\omega_1^2+\omega_2^2+\tilde{\omega}_1^2+\tilde{\omega}_2^2}{2}C(\mathbf{0}), \end{aligned} \tag{5.5}$$

and it starts from

$$\begin{aligned} M_2(z=0,\boldsymbol{x}_1,\boldsymbol{x}_2,\boldsymbol{y}_1,\boldsymbol{y}_2) &= \exp\Big(-\frac{|\boldsymbol{x}_1+\boldsymbol{y}_1|^2+|\boldsymbol{x}_2+\boldsymbol{y}_2|^2}{4r_0^2}\Big) \\ &\quad\times\exp\Big(-\frac{|\boldsymbol{x}_1-\boldsymbol{y}_1|^2+|\boldsymbol{x}_2-\boldsymbol{y}_2|^2}{4\rho_0^2}\Big). \end{aligned}$$

5.3. The scintillation regime. In this paper we address a regime which can be considered as a particular case of the paraxial white-noise regime: the scintillation regime. The scintillation regime is valid if the correlation length of the medium (i.e., the transverse correlation length of the Brownian field B) is smaller than the radius of the TRM and the size of the TRM elements. If the correlation length is our reference length, this means that in this regime the covariance function C^ε, the radius of the TRM r_0^ε, the TRM element size ρ_0^ε, and the propagation distance L^ε are of the form

$$C^\varepsilon(\boldsymbol{x}) = \varepsilon C(\boldsymbol{x}), \qquad r_0^\varepsilon = \frac{r_0}{\varepsilon}, \qquad \rho_0^\varepsilon = \frac{\rho_0}{\varepsilon}, \qquad L^\varepsilon = \frac{L}{\varepsilon}. \tag{5.6}$$

Here ε is a small dimensionless parameter, and we will study the limit $\varepsilon \to 0$.

Note that in section 5.7 we will address a slightly different version of the scintillation regime, which is (5.6) in which the size of the TRM elements is of the same order as the correlation length of the medium: $\rho_0^\varepsilon = \rho_0$.

5.4. The second-order moment in the scintillation regime. Let us consider the second-order moment (5.1) in the scintillation regime (5.6). We assume that the two frequencies are close to each other, and we parameterize them as

$$\omega = \omega_0 + \varepsilon\Omega, \qquad \tilde{\omega} = \omega_0 - \varepsilon\Omega.$$

We parameterize the two points $\boldsymbol{x}$ and $\boldsymbol{y}$ as

$$\boldsymbol{r} = \frac{\boldsymbol{x}+\boldsymbol{y}}{2}, \qquad \boldsymbol{q} = \boldsymbol{x}-\boldsymbol{y}.$$

We consider a long propagation distance of the form z/ε.

In the variables $(z/\varepsilon, \boldsymbol{q}, \boldsymbol{r})$ the function M_1^ε satisfies the equation

$$\frac{\partial M_1^\varepsilon}{\partial z} = \frac{ic_o}{\omega_0\varepsilon}\nabla_{\boldsymbol{r}}\cdot\nabla_{\boldsymbol{q}} M_1^\varepsilon - \frac{ic_o\Omega}{\omega_0^2}\big(\frac{1}{4}\Delta_{\boldsymbol{r}} + \Delta_{\boldsymbol{q}}\big)M_1^\varepsilon + \frac{\omega_0^2}{4c_o^2}\big(C(\boldsymbol{q}) - C(\boldsymbol{0})\big)M_1^\varepsilon,$$

starting from

$$M_1^\varepsilon(z=0,\boldsymbol{q},\boldsymbol{r}) = \exp\Big(-\varepsilon^2\frac{|\boldsymbol{r}|^2}{r_0^2} - \varepsilon^2\frac{|\boldsymbol{q}|^2}{4\rho_0^2}\Big),$$

and where we have not written terms of order ε. The Fourier transform (in $\boldsymbol{q}$ and $\boldsymbol{r}$) of the second-order moment of the paraxial Green's function is defined by

$$\hat{M}_1^\varepsilon\Big(\frac{z}{\varepsilon},\boldsymbol{\xi},\boldsymbol{\zeta}\Big) = \iint_{\mathbb{R}^2\times\mathbb{R}^2} M_1^\varepsilon\Big(\frac{z}{\varepsilon},\boldsymbol{q},\boldsymbol{r}\Big)\exp\big(-i\boldsymbol{q}\cdot\boldsymbol{\xi} - i\boldsymbol{r}\cdot\boldsymbol{\zeta}\big)d\boldsymbol{r}d\boldsymbol{q}. \tag{5.7}$$

It satisfies

$$\begin{aligned}\frac{\partial\hat{M}_1^\varepsilon}{\partial z} = &-\frac{ic_o}{\omega_0\varepsilon}\boldsymbol{\xi}\cdot\boldsymbol{\zeta}\hat{M}_1^\varepsilon + \frac{ic_o\Omega}{\omega_0^2}\left(\frac{1}{4}|\boldsymbol{\zeta}|^2 + |\boldsymbol{\xi}|^2\right)\hat{M}_1^\varepsilon\\ &+\frac{\omega_0^2}{4(2\pi)^2c_o^2}\int_{\mathbb{R}^2}\hat{C}(\boldsymbol{k})\Big[-\hat{M}_1^\varepsilon(\boldsymbol{\xi},\boldsymbol{\zeta}) + \hat{M}_1^\varepsilon(\boldsymbol{\xi}-\boldsymbol{k},\boldsymbol{\zeta})\Big]d\boldsymbol{k}.\end{aligned}$$

Let us absorb the rapid phase in the function

$$\widetilde{M}_1^\varepsilon\Big(\frac{z}{\varepsilon},\boldsymbol{\xi},\boldsymbol{\zeta}\Big) = \hat{M}_1^\varepsilon\Big(\frac{z}{\varepsilon},\boldsymbol{\xi},\boldsymbol{\zeta}\Big)\exp\Big(\frac{ic_oz}{\omega_0\varepsilon}\boldsymbol{\xi}\cdot\boldsymbol{\zeta}\Big). \tag{5.8}$$

In the scintillation regime the rescaled function $\widetilde{M}_1^\varepsilon$ satisfies the equation with fast phases

$$\begin{aligned}\frac{\partial\widetilde{M}_1^\varepsilon}{\partial z} = &\frac{ic_o\Omega}{\omega_0^2}\left(\frac{1}{4}|\boldsymbol{\zeta}|^2 + |\boldsymbol{\xi}|^2\right)\widetilde{M}_1^\varepsilon\\ &+\frac{\omega_0^2}{4(2\pi)^2c_o^2}\int_{\mathbb{R}^2}\hat{C}(\boldsymbol{k})\Big[-\widetilde{M}_1^\varepsilon(\boldsymbol{\xi},\boldsymbol{\zeta}) + \widetilde{M}_1^\varepsilon(\boldsymbol{\xi}-\boldsymbol{k},\boldsymbol{\zeta})e^{i\frac{c_oz}{\varepsilon\omega_0}\boldsymbol{k}\cdot\boldsymbol{\zeta}}\Big]d\boldsymbol{k},\end{aligned} \tag{5.9}$$

starting from

$$\widetilde{M}_1^\varepsilon(z=0,\boldsymbol{\xi},\boldsymbol{\zeta}) = (2\pi)^4\phi^\varepsilon_{\sqrt{2}\rho_0}(\boldsymbol{\xi})\phi^\varepsilon_{r_0/\sqrt{2}}(\boldsymbol{\zeta}), \tag{5.10}$$

where we have denoted

$$\phi_\rho^\varepsilon(\boldsymbol{\xi}) = \frac{\rho^2}{2\pi\varepsilon^2}\exp\Big(-\frac{\rho^2}{2\varepsilon^2}|\boldsymbol{\xi}|^2\Big). \tag{5.11}$$

Note that ϕ_ρ^ε belongs to L^1 and has a L^1-norm equal to one and that it behaves like a Dirac distribution as $\varepsilon \to 0$.

PROPOSITION 5.1. *The function* $\widetilde{M}_1^\varepsilon(z/\varepsilon, \boldsymbol{\xi}, \boldsymbol{\zeta})$ *defined by* (5.8) *can be expanded as*

$$\begin{aligned}\widetilde{M}_1^\varepsilon\left(\frac{z}{\varepsilon}, \boldsymbol{\xi}, \boldsymbol{\zeta}\right) &= K(z)\phi^\varepsilon_{\sqrt{2}\rho_0}(\boldsymbol{\xi})\phi^\varepsilon_{r_0/\sqrt{2}}(\boldsymbol{\zeta}) \\ &\quad + \phi^\varepsilon_{r_0/\sqrt{2}}(\boldsymbol{\zeta}) A\left(z, \boldsymbol{\xi}, \frac{\boldsymbol{\zeta}}{\varepsilon}, \Omega\right) + R_1^\varepsilon(z, \boldsymbol{\xi}, \boldsymbol{\zeta}),\end{aligned} \tag{5.12}$$

where the function K *is defined by*

$$K(z) = (2\pi)^4 \exp\Big(-\frac{\omega_0^2}{4c_o^2} C(\mathbf{0}) z\Big), \tag{5.13}$$

the function $(z, \boldsymbol{\xi}) \mapsto A(z, \boldsymbol{\xi}, \boldsymbol{\zeta}, \Omega)$ *is the solution of*

$$\begin{aligned}\partial_z A &= \frac{ic_o\Omega}{\omega_0^2}|\boldsymbol{\xi}|^2 A + \frac{\omega_0^2}{4(2\pi)^2 c_o^2}\int_{\mathbb{R}^2} \hat{C}(\boldsymbol{k})\big[A(\boldsymbol{\xi}-\boldsymbol{k})e^{\frac{ic_o z}{\omega_0}\boldsymbol{k}\cdot\boldsymbol{\zeta}} - A(\boldsymbol{\xi})\big]d\boldsymbol{k} \\ &\quad + \frac{\omega_0^2}{4(2\pi)^2 c_o^2} K(z)\hat{C}(\boldsymbol{\xi}) e^{\frac{ic_o z}{\omega_0}\boldsymbol{\xi}\cdot\boldsymbol{\zeta}},\end{aligned} \tag{5.14}$$

starting from $A(z=0, \boldsymbol{\xi}, \boldsymbol{\zeta}, \Omega) = 0$, *and the function* R_1^ε *satisfies*

$$\sup_{z\in[0,Z]} \|R_1^\varepsilon(z, \cdot, \cdot)\|_{L^1(\mathbb{R}^2\times\mathbb{R}^2)} \overset{\varepsilon\to 0}{\longrightarrow} 0 \tag{5.15}$$

for any $Z > 0$.

Proof. We introduce

$$\begin{aligned}\check{M}_1^\varepsilon(z, \boldsymbol{\xi}, \boldsymbol{\zeta}) &= \widetilde{M}_1^\varepsilon\left(\frac{z}{\varepsilon}, \boldsymbol{\xi}, \boldsymbol{\zeta}\right)\exp\left(-i\frac{c_o\Omega}{\omega_0^2}\left(\frac{1}{4}|\boldsymbol{\zeta}|^2 + |\boldsymbol{\xi}|^2\right)z\right), \\ \check{A}^\varepsilon(z, \boldsymbol{\xi}, \boldsymbol{\zeta}) &= A\left(z, \boldsymbol{\xi}, \frac{\boldsymbol{\zeta}}{\varepsilon}, \Omega\right)\exp\left(-i\frac{c_o\Omega}{\omega_0^2}|\boldsymbol{\xi}|^2 z\right).\end{aligned}$$

We first note that, for any $\boldsymbol{\zeta}$, we have using Bochner's theorem

$$\partial_z\|\check{A}^\varepsilon(z, \cdot, \boldsymbol{\zeta})\|_{L^1} \le \frac{\omega_0^2}{2c_o^2} C(\mathbf{0})\|\check{A}^\varepsilon(z, \cdot, \boldsymbol{\zeta})\|_{L^1} + \frac{\omega_0^2}{4c_o^2} K(z) C(\mathbf{0}),$$

which shows by Gronwall's lemma that

$$\sup_{z\in[0,Z], \boldsymbol{\zeta}\in\mathbb{R}^2} \partial_z\|\check{A}^\varepsilon(z, \cdot, \boldsymbol{\zeta})\|_{L^1} < \infty.$$

If we define the operator $\check{\mathcal{L}}^\varepsilon$ from $L^1(\mathbb{R}^2\times\mathbb{R}^2)$ to $L^1(\mathbb{R}^2\times\mathbb{R}^2)$

$$[\check{\mathcal{L}}^\varepsilon \check{M}](\boldsymbol{\xi}, \boldsymbol{\zeta}) = \frac{\omega_0^2}{4(2\pi)^2 c_o^2}\int_{\mathbb{R}^2} \hat{C}(\boldsymbol{k})\big[\check{M}(\boldsymbol{\xi}-\boldsymbol{k}, \boldsymbol{\zeta})e^{i\frac{c_o\Omega}{\omega_0^2}(|\boldsymbol{k}|^2 - 2\boldsymbol{\xi}\cdot\boldsymbol{k})z + i\frac{c_o}{\varepsilon\omega_0}\boldsymbol{k}\cdot\boldsymbol{\zeta} z} - \check{M}(\boldsymbol{\xi}, \boldsymbol{\zeta})\big]d\boldsymbol{k},$$

whose norm is bounded by $\|\check{\mathcal{L}}^\varepsilon\|_{L^1\to L^1} \le \frac{\omega_0^2}{2c_o^2} C(\mathbf{0})$, then we get from (5.9) that $\check{M}_1^\varepsilon$ satisfies the equation

$$\partial_z \check{M}_1^\varepsilon = \check{\mathcal{L}}^\varepsilon \check{M}_1^\varepsilon.$$

Denoting

$$\check{R}^\varepsilon(z,\boldsymbol{\xi},\boldsymbol{\zeta}) = \check{M}_1^\varepsilon(z,\boldsymbol{\xi},\boldsymbol{\zeta}) - \check{N}^\varepsilon(z,\boldsymbol{\xi},\boldsymbol{\zeta}),$$
$$\check{N}^\varepsilon(z,\boldsymbol{\xi},\boldsymbol{\zeta}) = K(z)\phi^\varepsilon_{\sqrt{2}\rho_0}(\boldsymbol{\xi})\phi^\varepsilon_{r_0/\sqrt{2}}(\boldsymbol{\zeta}) + \phi^\varepsilon_{r_0/\sqrt{2}}(\boldsymbol{\zeta})\check{A}^\varepsilon(z,\boldsymbol{\xi},\boldsymbol{\zeta}),$$

we have

$$\partial_z \check{R}^\varepsilon = \check{\mathcal{L}}^\varepsilon \check{R}^\varepsilon + \check{S}^\varepsilon, \tag{5.16}$$

with

$$\check{S}^\varepsilon(z,\boldsymbol{\xi},\boldsymbol{\zeta}) = -\partial_z \check{N}^\varepsilon(z,\boldsymbol{\xi},\boldsymbol{\zeta}) + \check{\mathcal{L}}^\varepsilon \check{N}^\varepsilon(z,\boldsymbol{\xi},\boldsymbol{\zeta}).$$

The function $\check{S}^\varepsilon$ is equal to

$$\check{S}^\varepsilon(z,\boldsymbol{\xi},\boldsymbol{\zeta}) = \frac{\omega_0^2}{4(2\pi)^2 c_o^2} K(z)\phi^\varepsilon_{r_0/\sqrt{2}}(\boldsymbol{\zeta}) e^{i\frac{c_o}{\omega_0\varepsilon}\boldsymbol{\xi}\cdot\boldsymbol{\zeta} z - i\frac{c_o\Omega}{\omega_0^2}|\boldsymbol{\xi}|^2 z}$$
$$\times\Big[\int_{\mathbb{R}^2} \hat{C}(\boldsymbol{\xi}-\boldsymbol{k})\phi^\varepsilon_{\sqrt{2}\rho_0}(\boldsymbol{k}) e^{-i\frac{c_o}{\omega_0\varepsilon}\boldsymbol{k}\cdot\boldsymbol{\zeta} z + i\frac{c_o\Omega}{\omega_0^2}|\boldsymbol{k}|^2 z} d\boldsymbol{k} - \hat{C}(\boldsymbol{\xi})\Big].$$

Its L^1-norm can be evaluated as follows for $z \in [0,Z]$:

$$\begin{aligned}
&\|\check{S}^\varepsilon(z,\cdot,\cdot)\|_{L^1} \\
&= \frac{\omega_0^2 K(z)}{4(2\pi)^2 c_o^2} \iint d\boldsymbol{\zeta} d\boldsymbol{\xi} \phi^1_{r_0/\sqrt{2}}(\boldsymbol{\zeta}) \Big| \int \hat{C}(\boldsymbol{\xi}-\varepsilon\boldsymbol{k})\phi^1_{\sqrt{2}\rho_0}(\boldsymbol{k}) e^{-i\varepsilon\frac{c_o}{\omega_0}\boldsymbol{k}\cdot\boldsymbol{\zeta} z + i\varepsilon^2\frac{c_o\Omega}{\omega_0^2}|\boldsymbol{k}|^2 z} d\boldsymbol{k} \\
&\quad - \hat{C}(\boldsymbol{\xi})\Big| \\
&\le \frac{\omega_0^2 K(z)}{4(2\pi)^2 c_o^2} \iiint d\boldsymbol{\zeta} d\boldsymbol{\xi} d\boldsymbol{k} \phi^1_{r_0/\sqrt{2}}(\boldsymbol{\zeta})\phi^1_{\sqrt{2}\rho_0}(\boldsymbol{k}) \Big| \hat{C}(\boldsymbol{\xi}-\varepsilon\boldsymbol{k}) e^{-i\varepsilon\frac{c_o}{\omega_0}\boldsymbol{k}\cdot\boldsymbol{\zeta} z + i\varepsilon^2\frac{c_o\Omega}{\omega_0^2}|\boldsymbol{k}|^2 z} - \hat{C}(\boldsymbol{\xi}) \Big| \\
&\le \frac{\omega_0^2 K(z)}{4(2\pi)^2 c_o^2} \iint d\boldsymbol{\zeta} d\boldsymbol{k} \phi^1_{r_0/\sqrt{2}}(\boldsymbol{\zeta})\phi^1_{\sqrt{2}\rho_0}(\boldsymbol{k}) \left[\int \big|\hat{C}(\boldsymbol{\xi}-\varepsilon\boldsymbol{k}) - \hat{C}(\boldsymbol{\xi})\big| d\boldsymbol{\xi}\right] \\
&\quad + \frac{\omega_0^2 K(z)}{4(2\pi)^2 c_o^2} \iiint d\boldsymbol{\zeta} d\boldsymbol{\xi} d\boldsymbol{k} \phi^1_{r_0/\sqrt{2}}(\boldsymbol{\zeta})\phi^1_{\sqrt{2}\rho_0}(\boldsymbol{k}) \hat{C}(\boldsymbol{\xi}) \big| e^{-i\varepsilon\frac{c_o}{\omega_0}\boldsymbol{k}\cdot\boldsymbol{\zeta} z + i\varepsilon^2\frac{c_o\Omega}{\omega_0^2}|\boldsymbol{k}|^2 z} - 1\big| \\
&\le \frac{\omega_0^2 (2\pi)^2}{4c_o^2} \int d\boldsymbol{k} \phi^1_{\sqrt{2}\rho_0}(\boldsymbol{k}) \left[\int \big|\hat{C}(\boldsymbol{\xi}-\varepsilon\boldsymbol{k}) - \hat{C}(\boldsymbol{\xi})\big| d\boldsymbol{\xi}\right] \\
&\quad + \frac{(2\pi)^4 \omega_0^2 C(\mathbf{0}) Z}{4c_o^2} \iint d\boldsymbol{\zeta} d\boldsymbol{k} \phi^1_{r_0/\sqrt{2}}(\boldsymbol{\zeta})\phi^1_{\sqrt{2}\rho_0}(\boldsymbol{k}) \left(\varepsilon\frac{c_o}{\omega_0}|\boldsymbol{k}||\boldsymbol{\zeta}| + \varepsilon^2\frac{c_o\Omega}{\omega_0^2}|\boldsymbol{k}|^2\right).
\end{aligned}$$

The term within the square brackets is bounded by $2(2\pi)^2 C(\mathbf{0})$ and goes to zero as $\varepsilon \to 0$ for any $\boldsymbol{k}$ (because $\hat{C} \in L^1$ and $\hat{C}$ is continuous, as it is the inverse Fourier transform of an L^1-function), so the first term of the right-hand side goes to zero as $\varepsilon \to 0$ by Lebesgue's dominated convergence theorem. The second term of the right-hand side is of order ε and it goes to zero as $\varepsilon \to 0$. As a result,

$$\sup_{z\in[0,Z]} \|\check{S}^\varepsilon(z,\cdot,\cdot)\|_{L^1} \overset{\varepsilon\to 0}{\longrightarrow} 0.$$

Integrating (5.16) and taking the L^1-norm, we find that for any $z \in [0,Z]$:

$$\|\check{R}^\varepsilon(z,\cdot,\cdot)\|_{L^1} \le \frac{\omega_0^2}{2c_o^2} C(\mathbf{0}) \int_0^z \|\check{R}^\varepsilon(z',\cdot,\cdot)\|_{L^1} dz' + \int_0^z \|\check{S}^\varepsilon(z',\cdot,\cdot)\|_{L^1} dz'.$$

Applying Gronwall's lemma gives

$$\sup_{z\in[0,Z]} \|\check{R}^\varepsilon(z,\cdot,\cdot)\|_{L^1} \overset{\varepsilon\to 0}{\longrightarrow} 0. \tag{5.17}$$

Finally, the residual R_1^ε defined by (5.12) can be expressed as

$$\begin{aligned} R_1^\varepsilon(z,\boldsymbol{\xi},\boldsymbol{\zeta}) = \check{R}^\varepsilon(z,\boldsymbol{\xi},\boldsymbol{\zeta}) \exp\left(i\frac{c_o\Omega}{\omega_0^2}\left(\frac{1}{4}|\boldsymbol{\zeta}|^2+|\boldsymbol{\xi}|^2\right)z\right) \\ + K(z)\phi^\varepsilon_{\sqrt{2}\rho_0}(\boldsymbol{\xi})\phi^\varepsilon_{r_0/\sqrt{2}}(\boldsymbol{\zeta})\Big[\exp\left(i\frac{c_o\Omega}{\omega_0^2}\left(\frac{1}{4}|\boldsymbol{\zeta}|^2+|\boldsymbol{\xi}|^2\right)z\right)-1\Big] \\ + \phi^\varepsilon_{r_0/\sqrt{2}}(\boldsymbol{\zeta})A\big(z,\boldsymbol{\xi},\frac{\boldsymbol{\zeta}}{\varepsilon},\Omega\big)\Big[\exp\left(i\frac{c_o\Omega}{\omega_0^2}\frac{1}{4}|\boldsymbol{\zeta}|^2 z\right)-1\Big]. \end{aligned}$$

The L^1-norm in $(\boldsymbol{\xi},\boldsymbol{\zeta})$ of the first term of the right-hand side goes to zero by (5.17). The L^1-norm of the second term is

$$\iint d\boldsymbol{\xi}d\boldsymbol{\zeta}K(z)\phi^1_{\sqrt{2}\rho_0}(\boldsymbol{\xi})\phi^1_{r_0/\sqrt{2}}(\boldsymbol{\zeta})\Big|\exp\left(i\frac{c_o\Omega\varepsilon^2}{\omega_0^2}\left(\frac{1}{4}|\boldsymbol{\zeta}|^2+|\boldsymbol{\xi}|^2\right)z\right)-1\Big|$$

which is bounded by

$$\frac{(2\pi)^4 c_o|\Omega|\varepsilon^2}{\omega_0^2}Z\iint d\boldsymbol{\xi}d\boldsymbol{\zeta}\phi^1_{\sqrt{2}\rho_0}(\boldsymbol{\xi})\phi^1_{r_0/\sqrt{2}}(\boldsymbol{\zeta})\left(\frac{1}{4}|\boldsymbol{\zeta}|^2+|\boldsymbol{\xi}|^2\right)$$

which goes to zero as $\varepsilon\to 0$. The L^1-norm of the third term is

$$\iint d\boldsymbol{\xi}d\boldsymbol{\zeta}\phi^1_{r_0/\sqrt{2}}(\boldsymbol{\zeta})|A(z,\boldsymbol{\xi},\boldsymbol{\zeta})|\Big|\exp\left(i\frac{c_o\Omega\varepsilon^2}{\omega_0^2}\frac{1}{4}|\boldsymbol{\zeta}|^2 z\right)-1\Big|$$

which is bounded by

$$\frac{c_o|\Omega|\varepsilon^2}{4\omega_0^2}Z\iint d\boldsymbol{\xi}d\boldsymbol{\zeta}\phi^1_{r_0/\sqrt{2}}(\boldsymbol{\zeta})|A(z,\boldsymbol{\xi},\boldsymbol{\zeta})||\boldsymbol{\zeta}|^2,$$

which goes to zero as $\varepsilon\to 0$ because $\sup_{z\in[0,Z],\boldsymbol{\zeta}\in\mathbb{R}^2}\|A(z,\cdot,\boldsymbol{\zeta})\|_{L^1}$ is bounded. This completes the proof of the proposition. ∎

We remark that A defined by (5.14) describes how energy is transferred from the coherent part to the incoherent part of the wave field and also in between different lateral slowness modes. The first term in the right-hand side of (5.14) captures the decorrelation due to frequency separation, the second term captures random forward scattering and transfer of incoherent energy between different lateral slowness modes, and the third term captures transfer of energy from the coherent part to the scattered part of the wave field.

5.5. The fourth-order moment in the scintillation regime. Let us consider the fourth-order moment (5.3) in the scintillation regime (5.6). We assume that the four frequencies are close to each other, and we parameterize them as

$$\omega_1 = \omega_0 + \varepsilon(\Omega_1 + \Omega_2 + \Omega_3), \qquad \omega_2 = \omega_0 + \varepsilon(-\Omega_1 + \Omega_2 - \Omega_3),$$
$$\tilde{\omega}_1 = \omega_0 + \varepsilon(\Omega_1 - \Omega_2 - \Omega_3), \qquad \tilde{\omega}_2 = \omega_0 + \varepsilon(-\Omega_1 - \Omega_2 + \Omega_3).$$

We parameterize the four points $\boldsymbol{x}_1, \boldsymbol{x}_2, \boldsymbol{y}_1, \boldsymbol{y}_2$ in (5.4) in the special way:

$$\boldsymbol{x}_1 = \frac{\boldsymbol{r}_1 + \boldsymbol{r}_2 + \boldsymbol{q}_1 + \boldsymbol{q}_2}{2}, \qquad \boldsymbol{y}_1 = \frac{\boldsymbol{r}_1 + \boldsymbol{r}_2 - \boldsymbol{q}_1 - \boldsymbol{q}_2}{2},$$
$$\boldsymbol{x}_2 = \frac{\boldsymbol{r}_1 - \boldsymbol{r}_2 + \boldsymbol{q}_1 - \boldsymbol{q}_2}{2}, \qquad \boldsymbol{y}_2 = \frac{\boldsymbol{r}_1 - \boldsymbol{r}_2 - \boldsymbol{q}_1 + \boldsymbol{q}_2}{2}.$$

We consider a long propagation distance of the form z/ε. In the variables $(z/\varepsilon, \boldsymbol{q}_1, \boldsymbol{q}_2, \boldsymbol{r}_1, \boldsymbol{r}_2)$ the function M_2^ε satisfies the equation

$$\begin{aligned}\frac{\partial M_2^\varepsilon}{\partial z} &= \frac{ic_o}{\omega_0\varepsilon}\big(\nabla_{\boldsymbol{r}_1}\cdot\nabla_{\boldsymbol{q}_1} + \nabla_{\boldsymbol{r}_2}\cdot\nabla_{\boldsymbol{q}_2}\big)M_2^\varepsilon - \frac{ic_o\Omega_1}{\omega_0^2}\big(\nabla_{\boldsymbol{r}_1}\cdot\nabla_{\boldsymbol{q}_2} + \nabla_{\boldsymbol{r}_2}\cdot\nabla_{\boldsymbol{q}_1}\big)M_2^\varepsilon \\ &\quad - \frac{ic_o\Omega_2}{2\omega_0^2}\big(\Delta_{\boldsymbol{r}_1} + \Delta_{\boldsymbol{r}_2} + \Delta_{\boldsymbol{q}_2} + \Delta_{\boldsymbol{q}_2}\big)M_2^\varepsilon - \frac{ic_o\Omega_3}{\omega_0^2}\big(\nabla_{\boldsymbol{r}_1}\cdot\nabla_{\boldsymbol{r}_2} + \nabla_{\boldsymbol{q}_1}\cdot\nabla_{\boldsymbol{q}_2}\big)M_2^\varepsilon \\ &\quad + \frac{\omega_0^2}{4c_o^2}\mathcal{U}_2(\boldsymbol{q}_1, \boldsymbol{q}_2, \boldsymbol{r}_1, \boldsymbol{r}_2)M_2^\varepsilon,\end{aligned} \tag{5.18}$$

with the generalized potential

$$\begin{aligned}\mathcal{U}_2(\boldsymbol{q}_1, \boldsymbol{q}_2, \boldsymbol{r}_1, \boldsymbol{r}_2) &= C(\boldsymbol{q}_2 + \boldsymbol{q}_1) + C(\boldsymbol{q}_2 - \boldsymbol{q}_1) + C(\boldsymbol{r}_2 + \boldsymbol{q}_1) + C(\boldsymbol{r}_2 - \boldsymbol{q}_1) \\ &\quad - C(\boldsymbol{q}_2 + \boldsymbol{r}_2) - C(\boldsymbol{q}_2 - \boldsymbol{r}_2) - 2C(\boldsymbol{0}),\end{aligned} \tag{5.19}$$

and where we have not written terms of order ε. The initial condition for (5.18) is

$$M_2^\varepsilon(z = 0, \boldsymbol{q}_1, \boldsymbol{q}_2, \boldsymbol{r}_1, \boldsymbol{r}_2) = \exp\Big(-\varepsilon^2\frac{|\boldsymbol{r}_1|^2 + |\boldsymbol{r}_2|^2}{2r_0^2} - \varepsilon^2\frac{|\boldsymbol{q}_1|^2 + |\boldsymbol{q}_2|^2}{2\rho_0^2}\Big).$$

The Fourier transform (in $\boldsymbol{q}_1$, $\boldsymbol{q}_2$, $\boldsymbol{r}_1$, and $\boldsymbol{r}_2$) of the fourth-order moment of the paraxial Green's function is defined by

$$\begin{aligned}\hat{M}_2^\varepsilon\Big(\frac{z}{\varepsilon}, \boldsymbol{\xi}_1, \boldsymbol{\xi}_2, \boldsymbol{\zeta}_1, \boldsymbol{\zeta}_2\Big) &= \iint_{\mathbb{R}^2\times\mathbb{R}^2\times\mathbb{R}^2\times\mathbb{R}^2} M_2^\varepsilon\Big(\frac{z}{\varepsilon}, \boldsymbol{q}_1, \boldsymbol{q}_2, \boldsymbol{r}_1, \boldsymbol{r}_2\Big) \\ &\quad \times \exp\big(-i\boldsymbol{q}_1\cdot\boldsymbol{\xi}_1 - i\boldsymbol{r}_1\cdot\boldsymbol{\zeta}_1 - i\boldsymbol{q}_2\cdot\boldsymbol{\xi}_2 - i\boldsymbol{r}_2\cdot\boldsymbol{\zeta}_2\big) \\ &\quad \times d\boldsymbol{r}_1 d\boldsymbol{r}_2 d\boldsymbol{q}_1 d\boldsymbol{q}_2.\end{aligned} \tag{5.20}$$

Let us absorb the rapid phase in the function

$$\widetilde{M}_2^\varepsilon\Big(\frac{z}{\varepsilon}, \boldsymbol{\xi}_1, \boldsymbol{\xi}_2, \boldsymbol{\zeta}_1, \boldsymbol{\zeta}_2\Big) = \hat{M}_2^\varepsilon\Big(\frac{z}{\varepsilon}, \boldsymbol{\xi}_1, \boldsymbol{\xi}_2, \boldsymbol{\zeta}_1, \boldsymbol{\zeta}_2\Big)\exp\Big(\frac{ic_o z}{\omega_0\varepsilon}(\boldsymbol{\xi}_2\cdot\boldsymbol{\zeta}_2 + \boldsymbol{\xi}_1\cdot\boldsymbol{\zeta}_1)\Big). \tag{5.21}$$

In the scintillation regime (5.6) the rescaled function $\widetilde{M}_2^\varepsilon$ satisfies the equation with fast phases

$$
\begin{aligned}
\frac{\partial \widetilde{M}_2^\varepsilon}{\partial z} &= \frac{ic_o\Omega_1}{\omega_0^2}\big(\boldsymbol{\xi}_1\cdot\boldsymbol{\zeta}_2+\boldsymbol{\xi}_2\cdot\boldsymbol{\zeta}_1\big)\widetilde{M}_2^\varepsilon \\
&+ \frac{ic_o\Omega_2}{2\omega_0^2}\big(|\boldsymbol{\xi}_1|^2+|\boldsymbol{\xi}_2|^2+|\boldsymbol{\zeta}_1|^2+|\boldsymbol{\zeta}_2|^2\big)\widetilde{M}_2^\varepsilon \\
&+ \frac{ic_o\Omega_3}{\omega_0^2}\big(\boldsymbol{\xi}_1\cdot\boldsymbol{\xi}_2+\boldsymbol{\zeta}_1\cdot\boldsymbol{\zeta}_2\big)\widetilde{M}_2^\varepsilon \\
&+ \frac{\omega_0^2}{4(2\pi)^2c_o^2}\int_{\mathbb{R}^2}\hat{C}(\boldsymbol{k})\Big[-2\widetilde{M}_2^\varepsilon(\boldsymbol{\xi}_1,\boldsymbol{\xi}_2,\boldsymbol{\zeta}_1,\boldsymbol{\zeta}_2) \\
&+ \widetilde{M}_2^\varepsilon(\boldsymbol{\xi}_1-\boldsymbol{k},\boldsymbol{\xi}_2-\boldsymbol{k},\boldsymbol{\zeta}_1,\boldsymbol{\zeta}_2)e^{i\frac{c_o z}{\varepsilon\omega_0}\boldsymbol{k}\cdot(\boldsymbol{\zeta}_2+\boldsymbol{\zeta}_1)} \\
&+ \widetilde{M}_2^\varepsilon(\boldsymbol{\xi}_1-\boldsymbol{k},\boldsymbol{\xi}_2,\boldsymbol{\zeta}_1,\boldsymbol{\zeta}_2-\boldsymbol{k})e^{i\frac{c_o z}{\varepsilon\omega_0}\boldsymbol{k}\cdot(\boldsymbol{\xi}_2+\boldsymbol{\zeta}_1)} \\
&+ \widetilde{M}_2^\varepsilon(\boldsymbol{\xi}_1+\boldsymbol{k},\boldsymbol{\xi}_2-\boldsymbol{k},\boldsymbol{\zeta}_1,\boldsymbol{\zeta}_2)e^{i\frac{c_o z}{\varepsilon\omega_0}\boldsymbol{k}\cdot(\boldsymbol{\zeta}_2-\boldsymbol{\zeta}_1)} \\
&+ \widetilde{M}_2^\varepsilon(\boldsymbol{\xi}_1+\boldsymbol{k},\boldsymbol{\xi}_2,\boldsymbol{\zeta}_1,\boldsymbol{\zeta}_2-\boldsymbol{k})e^{i\frac{c_o z}{\varepsilon\omega_0}\boldsymbol{k}\cdot(\boldsymbol{\xi}_2-\boldsymbol{\zeta}_1)} \\
&- \widetilde{M}_2^\varepsilon(\boldsymbol{\xi}_1,\boldsymbol{\xi}_2-\boldsymbol{k},\boldsymbol{\zeta}_1,\boldsymbol{\zeta}_2-\boldsymbol{k})e^{i\frac{c_o z}{\varepsilon\omega_0}(\boldsymbol{k}\cdot(\boldsymbol{\zeta}_2+\boldsymbol{\xi}_2)-|\boldsymbol{k}|^2)} \\
&- \widetilde{M}_2^\varepsilon(\boldsymbol{\xi}_1,\boldsymbol{\xi}_2-\boldsymbol{k},\boldsymbol{\zeta}_1,\boldsymbol{\zeta}_2+\boldsymbol{k})e^{i\frac{c_o z}{\varepsilon\omega_0}(\boldsymbol{k}\cdot(\boldsymbol{\zeta}_2-\boldsymbol{\xi}_2)+|\boldsymbol{k}|^2)}\Big]d\boldsymbol{k}, \qquad (5.22)
\end{aligned}
$$

starting from

$$
\widetilde{M}_2^\varepsilon(z=0,\boldsymbol{\xi}_1,\boldsymbol{\xi}_2,\boldsymbol{\zeta}_1,\boldsymbol{\zeta}_2)=(2\pi)^8\phi_{\rho_0}^\varepsilon(\boldsymbol{\xi}_1)\phi_{\rho_0}^\varepsilon(\boldsymbol{\xi}_2)\phi_{r_0}^\varepsilon(\boldsymbol{\zeta}_1)\phi_{r_0}^\varepsilon(\boldsymbol{\zeta}_2), \qquad (5.23)
$$

where ϕ_ρ^ε is defined by (5.11). The following result shows that $\widetilde{M}_2^\varepsilon$ exhibits a multiscale behavior as $\varepsilon\to 0$, with some components evolving at the scale ε and some components evolving at the order one scale.

PROPOSITION 5.2. *The function* $\widetilde{M}_2^\varepsilon(z/\varepsilon,\boldsymbol{\xi}_1,\boldsymbol{\xi}_2,\boldsymbol{\zeta}_1,\boldsymbol{\zeta}_2)$ *defined by* (5.21) *can be expanded as*

$$
\begin{aligned}
\widetilde{M}_2^\varepsilon\left(\frac{z}{\varepsilon},\boldsymbol{\xi}_1,\boldsymbol{\xi}_2,\boldsymbol{\zeta}_1,\boldsymbol{\zeta}_2\right) &= K(z)^2\phi_{\rho_0}^\varepsilon(\boldsymbol{\xi}_1)\phi_{\rho_0}^\varepsilon(\boldsymbol{\xi}_2)\phi_{r_0}^\varepsilon(\boldsymbol{\zeta}_1)\phi_{r_0}^\varepsilon(\boldsymbol{\zeta}_2) \\
&+ \frac{K(z)}{2}\phi_{\rho_0}^\varepsilon\left(\frac{\boldsymbol{\xi}_1-\boldsymbol{\xi}_2}{\sqrt{2}}\right)\phi_{r_0}^\varepsilon(\boldsymbol{\zeta}_1)\phi_{r_0}^\varepsilon(\boldsymbol{\zeta}_2)A\left(z,\frac{\boldsymbol{\xi}_2+\boldsymbol{\xi}_1}{2},\frac{\boldsymbol{\zeta}_2+\boldsymbol{\zeta}_1}{\varepsilon},\Omega_2+\Omega_3\right) \\
&+ \frac{K(z)}{2}\phi_{\rho_0}^\varepsilon\left(\frac{\boldsymbol{\xi}_1+\boldsymbol{\xi}_2}{\sqrt{2}}\right)\phi_{r_0}^\varepsilon(\boldsymbol{\zeta}_1)\phi_{r_0}^\varepsilon(\boldsymbol{\zeta}_2)A\left(z,\frac{\boldsymbol{\xi}_2-\boldsymbol{\xi}_1}{2},\frac{\boldsymbol{\zeta}_2-\boldsymbol{\zeta}_1}{\varepsilon},\Omega_2-\Omega_3\right) \\
&+ \frac{K(z)}{2}\phi_{R_0}^\varepsilon\left(\frac{\boldsymbol{\xi}_1-\boldsymbol{\zeta}_2}{\sqrt{2}}\right)\phi_{r_0}^\varepsilon(\boldsymbol{\zeta}_1)\phi_{\rho_0}^\varepsilon(\boldsymbol{\xi}_2)A\left(z,\frac{\boldsymbol{\zeta}_2+\boldsymbol{\xi}_1}{2},\frac{\boldsymbol{\xi}_2+\boldsymbol{\zeta}_1}{\varepsilon},\Omega_2+\Omega_1\right) \\
&+ \frac{K(z)}{2}\phi_{R_0}^\varepsilon\left(\frac{\boldsymbol{\xi}_1+\boldsymbol{\zeta}_2}{\sqrt{2}}\right)\phi_{r_0}^\varepsilon(\boldsymbol{\zeta}_1)\phi_{\rho_0}^\varepsilon(\boldsymbol{\xi}_2)A\left(z,\frac{\boldsymbol{\zeta}_2-\boldsymbol{\xi}_1}{2},\frac{\boldsymbol{\xi}_2-\boldsymbol{\zeta}_1}{\varepsilon},\Omega_2-\Omega_1\right) \\
&+ \frac{1}{4}\phi_{r_0}^\varepsilon(\boldsymbol{\zeta}_1)\phi_{r_0}^\varepsilon(\boldsymbol{\zeta}_2)A\left(z,\frac{\boldsymbol{\xi}_2+\boldsymbol{\xi}_1}{2},\frac{\boldsymbol{\zeta}_2+\boldsymbol{\zeta}_1}{\varepsilon},\Omega_2+\Omega_3\right) \\
&\quad\times A\left(z,\frac{\boldsymbol{\xi}_2-\boldsymbol{\xi}_1}{2},\frac{\boldsymbol{\zeta}_2-\boldsymbol{\zeta}_1}{\varepsilon},\Omega_2-\Omega_3\right) \\
&+ \frac{1}{4}\phi_{r_0}^\varepsilon(\boldsymbol{\zeta}_1)\phi_{\rho_0}^\varepsilon(\boldsymbol{\xi}_2)A\left(z,\frac{\boldsymbol{\zeta}_2+\boldsymbol{\xi}_1}{2},\frac{\boldsymbol{\xi}_2+\boldsymbol{\zeta}_1}{\varepsilon},\Omega_2+\Omega_1\right) \\
&\quad\times A\left(z,\frac{\boldsymbol{\zeta}_2-\boldsymbol{\xi}_1}{2},\frac{\boldsymbol{\xi}_2-\boldsymbol{\zeta}_1}{\varepsilon},\Omega_2-\Omega_1\right) \\
&+ R_2^\varepsilon(z,\boldsymbol{\xi}_1,\boldsymbol{\xi}_2,\boldsymbol{\zeta}_1,\boldsymbol{\zeta}_2), \qquad (5.24)
\end{aligned}
$$

where

$$\frac{1}{R_0^2} = \frac{1}{2}\Big(\frac{1}{r_0^2} + \frac{1}{\rho_0^2}\Big), \tag{5.25}$$

the function K is defined by (5.13), *the function $(z, \boldsymbol{\xi}) \mapsto A(z, \boldsymbol{\xi}, \boldsymbol{\zeta}, \Omega)$ is the solution of* (5.14), *and the function R_2^ε satisfies*

$$\sup_{z\in[0,Z]} \|R_2^\varepsilon(z,\cdot,\cdot,\cdot,\cdot)\|_{L^1(\mathbb{R}^2\times\mathbb{R}^2\times\mathbb{R}^2\times\mathbb{R}^2)} \stackrel{\varepsilon\to 0}{\longrightarrow} 0 \tag{5.26}$$

for any $Z > 0$.

This result is an extension of Proposition 1 in [15] in which the case $r_0 = \rho_0$ and $\Omega = 0$ is addressed (whose proof follows the same lines as the one of Proposition 5.2). It shows that, if we deal with an integral of $\widetilde{M}_2^\varepsilon$ against a bounded function, then we can replace $\widetilde{M}_2^\varepsilon$ by the right-hand side of (5.24) without the R_2^ε term up to a negligible error when ε is small. Note also that the result shows that the fourth-order moment M_2 can be expressed in terms of second-order moment A in (5.14) and in terms of the source field, which can be seen as a "quasi-Gaussian property" [15].

5.6. The strongly scattering regime. Our goal is to find an explicit expression of the function A defined by (5.14). The equation (5.14) for A (in which $\boldsymbol{\zeta}$ and Ω are frozen parameters) can be solved exactly when $\Omega = 0$:

$$A(z,\boldsymbol{\xi},\boldsymbol{\zeta},0) = \frac{K(z)}{(2\pi)^2}\int_{\mathbb{R}^2}\Big[\exp\Big(\frac{\omega_0^2}{4c_o^2}\int_0^z C\big(\boldsymbol{x}+\frac{c_o\boldsymbol{\zeta}}{\omega_0}z'\big)dz'\Big)-1\Big]\exp\big(-i\boldsymbol{\xi}\cdot\boldsymbol{x}\big)d\boldsymbol{x}. \tag{5.27}$$

When $\Omega \neq 0$ it is possible to find an approximate expression for $A(z, \boldsymbol{\xi}, \boldsymbol{\zeta}, \Omega)$ in the strongly scattering regime as we show below. The strongly scattering regime corresponds to

$$\omega_0^2 C(\mathbf{0}) L/c_o^2 \gg 1, \tag{5.28}$$

which means that the propagation distance L is larger than the scattering mean free path defined by

$$\ell_{\rm sca} = \frac{8c_o^2}{\omega_0^2 C(\mathbf{0})}. \tag{5.29}$$

Indeed, the scattering mean free path is the characteristic decay length of the mean Green's function, as shown by the form of the mean Green's function obtained by Itô's formula

$$\mathbb{E}[\hat{G}(\omega, L, \boldsymbol{x}, \boldsymbol{y})] = \hat{G}_0(\omega, L, \boldsymbol{x}, \boldsymbol{y}) \exp\Big(-\frac{\omega_0^2 C(\mathbf{0}) L}{8c_o^2}\Big),$$

where $\hat{G}_0$ is the homogeneous Green's function

$$\hat{G}_0(\omega, L, \boldsymbol{x}, \boldsymbol{y}) = \frac{\omega}{2i\pi c_o L}\exp\Big(i\frac{\omega|\boldsymbol{x}-\boldsymbol{y}|^2}{2c_o L}\Big);$$

see also the discussion in Appendix A.

We assume that the medium fluctuations are isotropic and smooth enough so that the coefficient

$$D = \frac{1}{(2\pi)^2}\int_{\mathbb{R}^2}\hat{C}(\boldsymbol{k})|\boldsymbol{k}|^2 d\boldsymbol{k} \tag{5.30}$$

is finite. The coefficient D is homogeneous to the inverse of a length. This length is the paraxial length; i.e., the propagation distance beyond which the paraxial approximation is not valid anymore. Indeed, in the strongly scattering regime $L \gg \ell_{\rm sca}$ (which is equivalent to $\omega_0^2 C(\mathbf{0})L/c_o^2 \gg 1$), the second moment of the Green's function is (see Proposition 12.7 in [12])

$$\mathbb{E}\big[\hat{G}(\omega, L, \boldsymbol{x}, \boldsymbol{y})\overline{\hat{G}(\omega, L, \boldsymbol{x}', \boldsymbol{y})}\big] = \hat{G}_0(\omega, L, \boldsymbol{x}, \boldsymbol{y})\overline{\hat{G}_0(\omega, L, \boldsymbol{x}', \boldsymbol{y})}\exp\Big(-\frac{|\boldsymbol{x}-\boldsymbol{x}'|^2}{X_c^2(L)}\Big),$$

where $X_c(L)$ is the correlation length of the wave field

$$X_c(L) = \frac{\sqrt{3}c_o}{\sqrt{D}\omega_0\sqrt{L}}. \tag{5.31}$$

When the correlation length of the field becomes of the order of the wavelength, i.e., when $\omega_0 X_c(L)/c_o \sim 1$, then the paraxial approximation is not valid anymore. The paraxial distance $\ell_{\rm par}$ such that $\omega_0 X_c(\ell_{\rm par})/c_o = 1$ is

$$\ell_{\rm par} = \frac{3}{D}. \tag{5.32}$$

Note that $\ell_{\rm par} \gg \ell_{\rm sca}$. The ratio $\ell_{\rm par}/\ell_{\rm sca}$ is of the order of the square of the ratio of the correlation length of the medium over the wavelength.

PROPOSITION 5.3. *When $L \gg \ell_{\rm sca}$, the function A solution of* (5.14) *can be approximated by the solution of the parabolic partial differential equation*

$$\partial_z A_{\rm s} = \frac{ic_o\Omega}{\omega_0^2}|\boldsymbol{\xi}|^2 A_{\rm s} + \frac{\omega_0^2 D}{16c_o^2}\Big[\Delta_{\boldsymbol{\xi}} A_{\rm s} - \frac{z^2c_o^2}{\omega_0^2}|\boldsymbol{\zeta}|^2 A_{\rm s} - 2i\frac{zc_o}{\omega_0}\boldsymbol{\zeta}\cdot\nabla_{\boldsymbol{\xi}} A_{\rm s}\Big], \tag{5.33}$$

starting from $A_{\rm s}(z=0,\boldsymbol{\xi},\boldsymbol{\zeta},\Omega) = (2\pi)^4\delta(\boldsymbol{\xi})$.

The approximation holds in the sense that, for any continuous and bounded function f and for any $Z > 0$:

$$\int_{\mathbb{R}^2} f(\boldsymbol{\xi})A(Z,\boldsymbol{\xi},\boldsymbol{\zeta},\Omega)d\boldsymbol{\xi} \overset{L\gg\ell_{\rm sca}}{\simeq} \int_{\mathbb{R}^2} f(\boldsymbol{\xi})A_{\rm s}(Z,\boldsymbol{\xi},\boldsymbol{\zeta},\Omega)d\boldsymbol{\xi}.$$

Proof. In the proof we assume that the correlation function of the medium is of the form $C^\delta(\boldsymbol{x}) = \delta^{-2}C(\delta\boldsymbol{x})$ and we study the convergence as $\delta \to 0$ of the solution of (5.14). Note that the corresponding coefficient $\ell_{\rm sca}^\delta$ defined by (5.29) is proportional to δ^2 while the corresponding coefficient D^δ defined by (5.30) is independent of δ in this scaling regime.

In the case $\Omega = 0$ the result can be obtained from the explicit expression (5.27). By taking the limit $\delta \to 0$ and using the expansion $C^\delta(\boldsymbol{x}) = \delta^{-2}C(\mathbf{0}) - D|\boldsymbol{x}|^2/4 + o(1)$, one gets the function

$$A_{\rm s}(z,\boldsymbol{\xi},\boldsymbol{\zeta},0) = (2\pi)^2\int_{\mathbb{R}^2}\exp\Big(-\frac{\omega_0^2 D}{16c_o^2}\int_0^z\Big|\boldsymbol{x}+\frac{c_o\boldsymbol{\zeta}}{\omega_0}z'\Big|dz' - i\boldsymbol{\xi}\cdot\boldsymbol{x}\Big)d\boldsymbol{x},$$

that is, the solution of (5.33) in the special case $\Omega = 0$.

In the general case $\Omega \neq 0$ we use a probabilistic representation and invoke a diffusion-approximation theorem. First, we introduce

$$\tilde{A}^\delta(z,\boldsymbol{\xi},\boldsymbol{\zeta},\Omega) = A^\delta(z,\boldsymbol{\xi},\boldsymbol{\zeta},\Omega)\exp\Big(-\frac{ic_o z}{\omega_0}\boldsymbol{\xi}\cdot\boldsymbol{\zeta}\Big) + (2\pi)^4\exp\Big(-\frac{\omega_0^2 C^\delta(\mathbf{0})z}{4c_o^2}\Big)\delta(\boldsymbol{\xi}).$$

It is the solution of

$$\partial_z \tilde{A}^\delta = \Big(\frac{ic_o\Omega}{\omega_0^2}|\boldsymbol{\xi}|^2 - \frac{ic_o}{\omega_0}\boldsymbol{\zeta}\cdot\boldsymbol{\xi}\Big)\tilde{A}^\delta + \frac{\omega_0^2}{4(2\pi)^2c_o^2}\int_{\mathbb{R}^2}\hat{C}^\delta(\boldsymbol{k})\big[\tilde{A}^\delta(\boldsymbol{\xi}-\boldsymbol{k}) - \tilde{A}^\delta(\boldsymbol{\xi})\big]d\boldsymbol{k},$$

starting from $\tilde{A}^\delta(z=0,\boldsymbol{\xi},\boldsymbol{\zeta},\Omega) = (2\pi)^4\delta(\boldsymbol{\xi})$. Second we define the operators

$$\mathcal{L}^\delta f(\boldsymbol{\xi}) = \frac{\omega_0^2}{4(2\pi)^2c_o^2}\int_{\mathbb{R}^2}\hat{C}^\delta(\boldsymbol{k})\big[f(\boldsymbol{\xi}-\boldsymbol{k}) - f(\boldsymbol{\xi})\big]d\boldsymbol{k}, \tag{5.34}$$

$$\mathcal{L}f(\boldsymbol{\xi}) = \frac{\omega_0^2 D}{16c_o^2}\Delta_{\boldsymbol{\xi}} f(\boldsymbol{\xi}). \tag{5.35}$$

Since $\hat{C}^\delta(\boldsymbol{k}) = \delta^{-4}\hat{C}(\boldsymbol{k}/\delta)$, the operator $\mathcal{L}^\delta$ can be written as

$$\mathcal{L}^\delta f(\boldsymbol{\xi}) = \frac{\omega_0^2}{4(2\pi)^2c_o^2\delta^2}\int_{\mathbb{R}^2}\hat{C}(\boldsymbol{k})\big[f(\boldsymbol{\xi}-\delta\boldsymbol{k}) - f(\boldsymbol{\xi})\big]d\boldsymbol{k},$$

and it is the infinitesimal generator of the random process $\boldsymbol{\Xi}^\delta(z) = \delta\,\boldsymbol{\Xi}(z/\delta^2)$ defined as

$$\boldsymbol{\Xi}(z) = \boldsymbol{\Xi}(0) + \sum_{k=1}^{N_z}\boldsymbol{k}_k,$$

where N_z is a homogeneous Poisson point process with intensity $\omega_0^2C(\mathbf{0})/(4c_o^2)$ and $(\boldsymbol{k}_k)_{k\geq 1}$ is a sequence of independent and identically distributed $\mathbb{R}^2$-valued random variables with the probability density function

$$p_{\boldsymbol{k}}(\boldsymbol{k}) = \frac{\hat{C}(\boldsymbol{k})}{(2\pi)^2C(\mathbf{0})}.$$

These random variables have mean zero and finite variance $D/C(\mathbf{0})$. The compound Poisson process $\boldsymbol{\Xi}$ has independent and stationary increments, with the distribution characterized by the characteristic function

$$\mathbb{E}\big[\exp\big(i\boldsymbol{x}\cdot(\boldsymbol{\Xi}(z'+z)-\boldsymbol{\Xi}(z'))\big)\big] = \exp\Big(\frac{\omega_0^2 z}{4c_o^2}\big(C(\boldsymbol{x})-C(\mathbf{0})\big)\Big). \tag{5.36}$$

Let us denote

$$V(\boldsymbol{\xi}) = \frac{c_o\Omega}{\omega_0^2}|\boldsymbol{\xi}|^2 - \frac{c_o}{\omega_0}\boldsymbol{\zeta}\cdot\boldsymbol{\xi}.$$

For any continuous and bounded function f and $Z>0$, the solution of

$$\partial_z\tilde{u}^\delta = iV(\boldsymbol{\xi})\tilde{u}^\delta - \mathcal{L}^\delta\tilde{u}^\delta,$$

with the terminal condition $\tilde{u}^\delta(z=Z,\boldsymbol{\xi}) = f(\boldsymbol{\xi})$, can be expressed by the Feynman–Kac formula as

$$\tilde{u}^\delta(z,\boldsymbol{\xi}) = \mathbb{E}\Big[f\big(\boldsymbol{\Xi}^\delta(Z)\big)\exp\Big(-i\int_z^Z V(\boldsymbol{\Xi}^\delta(z'))dz'\Big)\Big|\boldsymbol{\Xi}^\delta(z)=\boldsymbol{\xi}\Big].$$

We can check that

$$\partial_z \int_{\mathbb{R}^2} \overline{\tilde{u}^\delta(z,\boldsymbol{\xi})}\tilde{A}^\delta(z,\boldsymbol{\xi})d\boldsymbol{\xi} = 0;$$

therefore

$$\begin{aligned}\int_{\mathbb{R}^2} \overline{f(\boldsymbol{\xi})}\tilde{A}^\delta(Z,\boldsymbol{\xi})d\boldsymbol{\xi} &= \int_{\mathbb{R}^2} \overline{\tilde{u}^\delta(Z,\boldsymbol{\xi})}\tilde{A}^\delta(Z,\boldsymbol{\xi})d\boldsymbol{\xi} = \int_{\mathbb{R}^2} \overline{\tilde{u}^\delta(0,\boldsymbol{\xi})}\tilde{A}^\delta(0,\boldsymbol{\xi})d\boldsymbol{\xi}\\ &= (2\pi)^4\tilde{u}^\delta(0,\mathbf{0}).\end{aligned}$$

By Donsker's invariance principle the random process $\boldsymbol{\Xi}^\delta$ weakly converges (as a cadlag process) to a Brownian motion $\boldsymbol{W}$ with generator $\mathcal{L}$. This shows that $\tilde{u}^\delta(0,\mathbf{0})$ converges to $\tilde{u}(0,\mathbf{0})$, where $\tilde{u}(z,\boldsymbol{\xi})$ is defined by

$$\tilde{u}(z,\boldsymbol{\xi}) = \mathbb{E}\Big[f\big(\boldsymbol{W}(Z)\big)\exp\Big(-i\int_z^Z V(\boldsymbol{W}(z'))dz'\Big)\Big|\boldsymbol{W}(z)=\boldsymbol{\xi}\Big],$$

which is solution of

$$\partial_z\tilde{u} = iV(\boldsymbol{\xi})\tilde{u} - \mathcal{L}\tilde{u},$$

with the terminal condition $\tilde{u}(z=Z,\boldsymbol{\xi}) = f(\boldsymbol{\xi})$. If we denote by $\tilde{A}$ the solution of

$$\partial_z\tilde{A} = iV(\boldsymbol{\xi})\tilde{A} + \mathcal{L}\tilde{A},$$

with the initial condition $\tilde{A}(z=0,\boldsymbol{\xi}) = (2\pi)^4\delta(\boldsymbol{\xi})$, then we find that

$$\int_{\mathbb{R}^2} \overline{f(\boldsymbol{\xi})}\tilde{A}(Z,\boldsymbol{\xi})d\boldsymbol{\xi} = \int_{\mathbb{R}^2} \overline{\tilde{u}(Z,\boldsymbol{\xi})}\tilde{A}(Z,\boldsymbol{\xi})d\boldsymbol{\xi} = \int_{\mathbb{R}^2} \overline{\tilde{u}(0,\boldsymbol{\xi})}\tilde{A}(0,\boldsymbol{\xi})d\boldsymbol{\xi} = (2\pi)^4\tilde{u}(0,\mathbf{0}).$$

This establishes that, for any continuous and bounded function f and $Z>0$,

$$\int_{\mathbb{R}^2} \overline{f(\boldsymbol{\xi})}\tilde{A}^\delta(Z,\boldsymbol{\xi})d\boldsymbol{\xi} \overset{\delta\to 0}{\longrightarrow} \int_{\mathbb{R}^2} \overline{f(\boldsymbol{\xi})}\tilde{A}(Z,\boldsymbol{\xi})d\boldsymbol{\xi},$$

which proves that $\tilde{A}^\delta$ converges to $\tilde{A}$. By considering $A_{\mathrm{s}}(z,\boldsymbol{\xi}) = \tilde{A}(z,\boldsymbol{\xi})\exp\big(\frac{ic_o z}{\omega_0}\boldsymbol{\xi}\cdot\boldsymbol{\zeta}\big)$ we find that A_{s} satisfies (5.33), and A^δ converges to A_{s}, which is the desired result. ∎

Let us consider the partial inverse Fourier transform

$$\hat{A}_{\mathrm{s}}(z,\boldsymbol{x},\boldsymbol{\zeta},\Omega) = \frac{1}{(2\pi)^2}\int_{\mathbb{R}^2} A_{\mathrm{s}}(z,\boldsymbol{\xi},\boldsymbol{\zeta},\Omega)\exp(i\boldsymbol{\xi}\cdot\boldsymbol{x})d\boldsymbol{\xi}. \tag{5.37}$$

Proposition 5.4. *The partial inverse Fourier transform $\hat{A}_{\mathrm{s}}(z,\boldsymbol{x},\boldsymbol{\zeta},\Omega)$ has the form*

$$\hat{A}_{\mathrm{s}}(z,\boldsymbol{x},\boldsymbol{\zeta},\Omega) = (2\pi)^2\exp\big[-a_\Omega(z) - b_\Omega(z)|\boldsymbol{x}|^2 - c_\Omega(z)\boldsymbol{x}\cdot\boldsymbol{\zeta} - d_\Omega(z)|\boldsymbol{\zeta}|^2\big], \tag{5.38}$$

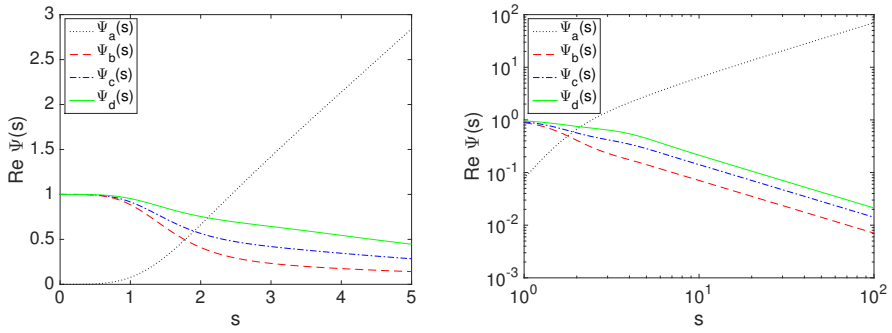

FIG. 5.1. *Real values of the functions $\Psi_{a,b,c,d}$ in linear scale (left) and log scale (right).*

where

$$a_\Omega(z) = \Psi_a\left(\sqrt{\frac{D\Omega}{4c_o}}z\right), \tag{5.39}$$

$$b_\Omega(z) = \frac{\omega_0^2 Dz}{16c_o^2}\Psi_b\left(\sqrt{\frac{D\Omega}{4c_o}}z\right), \tag{5.40}$$

$$c_\Omega(z) = \frac{\omega_0 Dz^2}{16c_o}\Psi_c\left(\sqrt{\frac{D\Omega}{4c_o}}z\right), \tag{5.41}$$

$$d_\Omega(z) = \frac{Dz^3}{48}\Psi_d\left(\sqrt{\frac{D\Omega}{4c_o}}z\right), \tag{5.42}$$

with the functions $\Psi_{a,b,c,d}$ defined by

$$\Psi_a(s) = \ln\Big[\cosh\left(e^{-i\frac{\pi}{4}}s\right)\Big], \tag{5.43}$$

$$\Psi_b(s) = \frac{\tanh(e^{-i\frac{\pi}{4}}s)}{e^{-i\frac{\pi}{4}}s}, \tag{5.44}$$

$$\Psi_c(s) = 2i\frac{e^{-i\frac{\pi}{4}}s\tanh(e^{-i\frac{\pi}{4}}s) - 1 + \cosh^{-1}(e^{-i\frac{\pi}{4}}s)}{s^2}, \tag{5.45}$$

$$\Psi_d(s) = 1 - \frac{3i}{s^3}\int_0^s \left(e^{-i\frac{\pi}{4}}s'\tanh(e^{-i\frac{\pi}{4}}s') - 1 + (\cosh(e^{-i\frac{\pi}{4}}s'))^{-1}\right)^2 ds'. \tag{5.46}$$

The real parts of the functions $\Psi_{a,b,c,d}$ are plotted in Figure 5.1. Note that they are positive valued. By Propositions 5.1 and 5.2 this result gives a complete and explicit expression of the second-order and fourth-order moments in the strongly scattering regime $L \gg \ell_{\rm sca}$.

Proof. By Proposition 5.3, $\hat{A}_{\rm s}$ is solution of

$$\partial_z \hat{A}_{\rm s} = -\frac{ic_o\Omega}{\omega_0^2}\Delta_{\boldsymbol{x}}\hat{A}_{\rm s} - \frac{\omega_0^2 D}{16c_o^2}\Big[|\boldsymbol{x}|^2 + \frac{z^2c_o^2}{\omega_0^2}|\boldsymbol{\zeta}|^2 + 2\frac{zc_o}{\omega_0}\boldsymbol{\zeta}\cdot\boldsymbol{x}\Big]\hat{A}_{\rm s},$$

starting from $\hat{A}_{\rm s}(z=0,\boldsymbol{x},\boldsymbol{\zeta},\Omega) = (2\pi)^2$. The solution has the form (5.38), where $(a_\Omega, b_\Omega, c_\Omega, d_\Omega)$ is the solution of the system of ordinary differential equations:

$$\frac{\mathrm{d}a_\Omega}{\mathrm{d}z} = -i\frac{4c_o\Omega}{\omega_0^2}b_\Omega, \tag{5.47}$$

$$\frac{\mathrm{d}b_\Omega}{\mathrm{d}z} = \frac{\omega_0^2 D}{16c_o^2} + i\frac{4c_o\Omega}{\omega_0^2}b_\Omega^2, \tag{5.48}$$

$$\frac{\mathrm{d}c_\Omega}{\mathrm{d}z} = \frac{\omega_0 D z}{8c_o} + i\frac{4c_o\Omega}{\omega_0^2}b_\Omega c_\Omega, \tag{5.49}$$

$$\frac{\mathrm{d}d_\Omega}{\mathrm{d}z} = \frac{Dz^2}{16} + i\frac{c_o\Omega}{\omega_0^2}c_\Omega^2, \tag{5.50}$$

starting from $(a_\Omega, b_\Omega, c_\Omega, d_\Omega)(z=0) = (0,0,0,0)$. We have $(a_{-\Omega}, b_{-\Omega}, c_{-\Omega}, d_{-\Omega})(z) = (\overline{a_\Omega}, \overline{b_\Omega}, \overline{c_\Omega}, \overline{d_\Omega})(z)$, and by solving the system, we obtain the desired result. ∎

When $D\Omega z^2/c_o \ll 1$, we can use Taylor series expansions of the functions $\Psi_{a,b,c,d}$ to obtain

$$\begin{aligned}
a_\Omega(z) &\simeq -i\frac{D\Omega z^2}{8c_o} + \frac{D^2\Omega^2 z^4}{192c_o^2} + O\Big(\frac{D^3\Omega^3 z^6}{c_o^3}\Big),\\
b_\Omega(z) &\simeq \frac{\omega_0^2 D z}{16c_o^2}\Big(1 + i\frac{D\Omega z^2}{12c_o} - \frac{D^2\Omega^2 z^4}{120c_o^2} + O\Big(\frac{D^3\Omega^3 z^6}{c_o^3}\Big)\Big),\\
c_\Omega(z) &\simeq \frac{\omega_0 D z^2}{16c_o}\Big(1 + i\frac{D\Omega z^2}{16c_o} - \frac{7D^2\Omega^2 z^4}{1152c_o^2} + O\Big(\frac{D^3\Omega^3 z^6}{c_o^3}\Big)\Big),\\
d_\Omega(z) &\simeq \frac{Dz^3}{48}\Big(1 + i\frac{3D\Omega z^2}{80c_o} - \frac{3D^2\Omega^2 z^4}{896c_o^2} + O\Big(\frac{D^3\Omega^3 z^6}{c_o^3}\Big)\Big).
\end{aligned}$$

The leading-order terms (with $\Omega = 0$) are consistent with the limit of (5.27) in the strongly scattering regime $L \gg \ell_{\mathrm{sca}}$.

When $D\Omega z^2/c_o \gg 1$, we can use asymptotic expressions for the functions $\Psi_{a,b,c,d}$ to obtain

$$\begin{aligned}
a_\Omega(z) &\simeq e^{-i\frac{\pi}{4}}\sqrt{\frac{D\Omega}{4c_o}}z - \ln 2,\\
b_\Omega(z) &\simeq e^{i\frac{\pi}{4}}\sqrt{\frac{\omega_0^4 D}{64c_o^3\Omega}},\\
c_\Omega(z) &\simeq e^{i\frac{\pi}{4}}\sqrt{\frac{\omega_0^2 D}{16c_o\Omega}}z - \frac{i\omega_0}{2\Omega},\\
d_\Omega(z) &\simeq e^{i\frac{\pi}{4}}\sqrt{\frac{c_o D}{64\Omega}}z^2 - \frac{ic_o z}{4\Omega} - e^{3i\frac{\pi}{4}}\sqrt{\frac{c_o^3}{4D\Omega^3}},
\end{aligned}$$

up to terms of relative order $\exp(-\sqrt{D\Omega/(8c_o)}z)$. Note that, for the asymptotic expansion of d_Ω, we used the fact that $\int_0^\infty 2(s-1)[s(\tanh(s) - s + \cosh^{-1}(s)] + [s(\tanh(s) - s + \cosh^{-1}(s)]^2 ds = 1$ in order to compute the $O(1)$-term. Compared to the small (or vanishing) Ω case, we can see that the growth rate in z of the coefficients are very different. This will have dramatic impact in the analysis of the refocused wave that we carry out in the next sections.

5.7. The scintillation regime revisited. In the scintillation regime (5.6) addressed in the previous section, the TRM element size ρ_0^ε is assumed to be of order ε^{-1}, that is to say, larger than the correlation length of the medium. We can also address the case where the TRM element size ρ_0^ε is of the same order as the correlation length of the medium:

$$C^\varepsilon(\boldsymbol{x}) = \varepsilon C(\boldsymbol{x}), \qquad r_0^\varepsilon = \frac{r_0}{\varepsilon}, \qquad \rho_0^\varepsilon = \rho_0, \qquad L^\varepsilon = \frac{L}{\varepsilon}. \tag{5.51}$$

The previous analysis can be revisited in the revised scintillation regime (5.51) and we get the following results.

PROPOSITION 5.5. *In the scintillation regime* (5.51), *the function* $\widetilde{M}_1^\varepsilon(z/\varepsilon, \boldsymbol{\xi}, \boldsymbol{\zeta})$ *defined by* (5.8) *can be expanded as*

$$\widetilde{M}_1^\varepsilon\left(\frac{z}{\varepsilon}, \boldsymbol{\xi}, \boldsymbol{\zeta}\right) = \phi^\varepsilon_{r_0/\sqrt{2}}(\boldsymbol{\zeta}) A\left(z, \boldsymbol{\xi}, \frac{\boldsymbol{\zeta}}{\varepsilon}, \Omega\right) + R_1^\varepsilon(z, \boldsymbol{\xi}, \boldsymbol{\zeta}),$$

where the function $(z, \boldsymbol{\xi}) \mapsto A(z, \boldsymbol{\xi}, \boldsymbol{\zeta}, \Omega)$ *is the solution of*

$$\partial_z A = \frac{ic_o\Omega}{\omega_0^2}|\boldsymbol{\xi}|^2 A + \frac{\omega_0^2}{4(2\pi)^2 c_o^2}\int_{\mathbb{R}^2} \hat{C}(\boldsymbol{k})\big[A(\boldsymbol{\xi}-\boldsymbol{k}) e^{\frac{ic_o z}{\omega_0}\boldsymbol{k}\cdot\boldsymbol{\zeta}} - A(\boldsymbol{\xi})\big] d\boldsymbol{k}, \tag{5.52}$$

starting from $A(z=0, \boldsymbol{\xi}, \boldsymbol{\zeta}, \Omega) = (2\pi)^4 \phi^1_{\sqrt{2}\rho_0}(\boldsymbol{\xi})$, *and the function* R_1^ε *satisfies*

$$\sup_{z\in[0,Z]} \|R_1^\varepsilon(z,\cdot,\cdot)\|_{L^1(\mathbb{R}^2\times\mathbb{R}^2)} \overset{\varepsilon\to 0}{\longrightarrow} 0 \tag{5.53}$$

for any $Z > 0$.

In particular, we have

$$\begin{aligned} &A(z, \boldsymbol{\xi}, \boldsymbol{\zeta}, 0) \\ &= (2\pi)^4 \int_{\mathbb{R}^2} \exp\left(-\frac{|\boldsymbol{x}|^2}{4\rho_0^2} + \frac{\omega_0^2}{4c_o^2}\int_0^z C\left(\boldsymbol{x} + \frac{c_o\boldsymbol{\zeta}z'}{\omega_0}\right) - C(\boldsymbol{0}) dz' - i\boldsymbol{\xi}\cdot\boldsymbol{x}\right) d\boldsymbol{x}. \end{aligned} \tag{5.54}$$

PROPOSITION 5.6. *In the scintillation regime* (5.51), *the function* $\widetilde{M}_2^\varepsilon(z/\varepsilon, \boldsymbol{\xi}_1, \boldsymbol{\xi}_2, \boldsymbol{\zeta}_1, \boldsymbol{\zeta}_2)$ *defined by* (5.21) *can be expanded as*

$$\begin{aligned} \widetilde{M}_2^\varepsilon\left(\frac{z}{\varepsilon}, \boldsymbol{\xi}_1, \boldsymbol{\xi}_2, \boldsymbol{\zeta}_1, \boldsymbol{\zeta}_2\right) =& \frac{1}{4}\phi^\varepsilon_{r_0}(\boldsymbol{\zeta}_1)\phi^\varepsilon_{r_0}(\boldsymbol{\zeta}_2) A\left(z, \frac{\boldsymbol{\xi}_2+\boldsymbol{\xi}_1}{2}, \frac{\boldsymbol{\zeta}_2+\boldsymbol{\zeta}_1}{\varepsilon}, \Omega_2+\Omega_3\right) \\ &\times A\left(z, \frac{\boldsymbol{\xi}_2-\boldsymbol{\xi}_1}{2}, \frac{\boldsymbol{\zeta}_2-\boldsymbol{\zeta}_1}{\varepsilon}, \Omega_2-\Omega_3\right) \\ &+ R_2^\varepsilon(z, \boldsymbol{\xi}_1, \boldsymbol{\xi}_2, \boldsymbol{\zeta}_1, \boldsymbol{\zeta}_2), \end{aligned} \tag{5.55}$$

where the function $(z, \boldsymbol{\xi}) \mapsto A(z, \boldsymbol{\xi}, \boldsymbol{\zeta}, \Omega)$ *is the solution of* (5.52), *and the function* R_2^ε *satisfies*

$$\sup_{z\in[0,Z]} \|R_2^\varepsilon(z,\cdot,\cdot,\cdot,\cdot)\|_{L^1(\mathbb{R}^2\times\mathbb{R}^2\times\mathbb{R}^2\times\mathbb{R}^2)} \overset{\varepsilon\to 0}{\longrightarrow} 0 \tag{5.56}$$

for any $Z > 0$.

In the strongly scattering regime $L \gg \ell_{\rm sca}$, Proposition 5.3 is still valid except that the initial condition for $A_{\rm s}$ is $A_{\rm s}(z=0,\boldsymbol{\xi},\boldsymbol{\zeta},\Omega) = (2\pi)^4 \phi^1_{\sqrt{2}\rho_0}(\boldsymbol{\xi})$ instead of $A_{\rm s}(z=0,\boldsymbol{\xi},\boldsymbol{\zeta},\Omega) = (2\pi)^4\delta(\boldsymbol{\xi})$. As a result, the expression of $\hat{A}_{\rm s}$ given in Proposition 5.4 has to be updated. The updated result is given in the following proposition.

PROPOSITION 5.7. *The partial inverse Fourier transform* $\hat{A}_{\rm s}(z,\boldsymbol{x},\boldsymbol{\zeta},\Omega)$ *has the form* (5.38), *where* $(a_\Omega, b_\Omega, c_\Omega, d_\Omega)$ *are given by* (5.39)–(5.42) *and the functions* $\Psi_{a,b,c,d}$ *are defined by*

$$\Psi_a(s) = \ln\Big[\cosh\left(e^{-i\frac{\pi}{4}}s\right) + T_0 \sinh\left(e^{-i\frac{\pi}{4}}s\right)\Big], \tag{5.57}$$

$$\Psi_b(s) = \frac{T_0 + \tanh(e^{-i\frac{\pi}{4}}s)}{e^{-i\frac{\pi}{4}}s[1+T_0\tanh(e^{-i\frac{\pi}{4}}s)]}, \tag{5.58}$$

$$\Psi_c(s) = 2i\frac{e^{-i\frac{\pi}{4}}s\frac{T_0+\tanh(e^{-i\frac{\pi}{4}}s)}{1+T_0\tanh(e^{-i\frac{\pi}{4}}s)} - 1 + \left[\cosh(e^{-i\frac{\pi}{4}}s) + T_0\sinh(e^{-i\frac{\pi}{4}}s)\right]^{-1}}{s^2}, \tag{5.59}$$

$$\Psi_d(s) = 1 - \frac{3i}{s^3}\int_0^s \left(e^{-i\frac{\pi}{4}}s'\frac{T_0+\tanh(e^{-i\frac{\pi}{4}}s')}{1+T_0\tanh(e^{-i\frac{\pi}{4}}s')} - 1 + \left[\cosh(e^{-i\frac{\pi}{4}}s') + T_0\sinh(e^{-i\frac{\pi}{4}}s')\right]^{-1}\right)^2 ds', \tag{5.60}$$

with

$$T_0 = \frac{2e^{-i\frac{\pi}{4}}}{\omega_0^2\rho_0^2}\sqrt{\frac{c_o^3\Omega}{D}}. \tag{5.61}$$

When $\rho_0 \to +\infty$, we have $T_0 = 0$, and we recover the result of Proposition 5.4.

Proof. $\hat{A}_{\rm s}$ is given by (5.38), and the functions $(a_\Omega, b_\Omega, c_\Omega, d_\Omega)$ satisfy the system of differential equations (5.47)–(5.50), with the initial condition $b_\Omega(0) = 1/(4\rho_0^2)$ instead of $b_\Omega(0) = 0$. By solving the differential equations we get the desired result. ∎

We remark that when $\Omega = 0$, we have

$$a_0(z) = 0, \quad b_0(z) = \frac{\omega_0^2 D z}{16 c_o^2} + \frac{1}{4\rho_0^2}, \quad c_o(z) = \frac{\omega_0 D z^2}{16 c_o}, \quad d_0(z) = \frac{D z^3}{48}. \tag{5.62}$$

6. Time-harmonic wave refocusing.

We address the situation described in section 3.1 in the scintillation regime (5.6). We consider two nearby frequencies $\omega = \omega_0 + \varepsilon\Omega$ and $\tilde{\omega} = \omega_0 - \varepsilon\Omega$. The goal is to determine the profile of the refocused wave and its SNR. We also want to determine for which frequency offset Ω time-reversal refocusing is still effective.

6.1. The mean refocused wave.

We first give the general expression of the mean refocused field in the scintillation regime.

PROPOSITION 6.1. *In the scintillation regime* (5.6) *the mean refocused field is*

$$\mathbb{E}\left[\hat{u}_{\rm tr}\left(\frac{\boldsymbol{y}}{\varepsilon}+\boldsymbol{x};\frac{\boldsymbol{y}}{\varepsilon}\right)\right] \stackrel{\varepsilon\to 0}{\longrightarrow} \frac{K(L)}{(2\pi)^4}\int \frac{r_0^2}{4\pi}\exp\Big(-\frac{r_0^2|\boldsymbol{\zeta}|^2}{4}+i\boldsymbol{y}\cdot\boldsymbol{\zeta}\Big)d\boldsymbol{\zeta}$$
$$+\frac{1}{(2\pi)^4}\iint_{\mathbb{R}^2\times\mathbb{R}^2}\frac{r_0^2}{4\pi}\exp\Big(-\frac{r_0^2|\boldsymbol{\zeta}|^2}{4}+i\boldsymbol{x}\cdot\boldsymbol{\xi}+i\boldsymbol{y}\cdot\boldsymbol{\zeta}-i\frac{Lc_o}{\omega_0}\boldsymbol{\xi}\cdot\boldsymbol{\zeta}\Big)A(L,\boldsymbol{\xi},\boldsymbol{\zeta},\Omega)d\boldsymbol{\xi}d\boldsymbol{\zeta}.$$

Proof. By using (5.1) and by taking $C\to\varepsilon C$, $r_0\to r_0/\varepsilon$, $\rho_0\to\rho_0/\varepsilon$, $\boldsymbol{y}\to\boldsymbol{y}/\varepsilon$, $L\to L/\varepsilon$, the mean refocused wave is given by

$$\begin{aligned}\mathbb{E}\left[\hat{u}_{\rm tr}\left(\frac{\boldsymbol{y}}{\varepsilon}+\boldsymbol{x};\frac{\boldsymbol{y}}{\varepsilon}\right)\right] &= \mathcal{M}_1\left(\frac{\boldsymbol{y}}{\varepsilon}+\boldsymbol{x},\frac{\boldsymbol{y}}{\varepsilon}\right)\\ &= M_1^\varepsilon\left(\frac{L}{\varepsilon},\boldsymbol{r}=\frac{\boldsymbol{y}}{\varepsilon}+\frac{\boldsymbol{x}}{2},\boldsymbol{q}=\boldsymbol{x}\right)\\ &= \frac{1}{(2\pi)^4}\iint_{\mathbb{R}^2\times\mathbb{R}^2}\widetilde{M}_1^\varepsilon\left(\frac{L}{\varepsilon},\boldsymbol{\xi},\boldsymbol{\zeta}\right)\\ &\quad\times\exp\left(i\boldsymbol{x}\cdot\boldsymbol{\xi}+i(\frac{\boldsymbol{y}}{\varepsilon}+\frac{\boldsymbol{x}}{2})\cdot\boldsymbol{\zeta}-i\frac{Lc_o}{\varepsilon\omega_0}\boldsymbol{\xi}\cdot\boldsymbol{\zeta}\right)d\boldsymbol{\xi}d\boldsymbol{\zeta}.\end{aligned}$$

In the limit $\varepsilon\to 0$, we find from Proposition 5.1 the desired result. ∎

In the weakly scattering regime $L\ll\ell_{\rm sca}$ (which is equivalent to $\omega_0^2C(\mathbf{0})L/c_o^2\ll 1$), we have $K(L)\simeq(2\pi)^4$ and $A\simeq 0$ so

$$\mathbb{E}\left[\hat{u}_{\rm tr}\left(\frac{\boldsymbol{y}}{\varepsilon}+\boldsymbol{x};\frac{\boldsymbol{y}}{\varepsilon}\right)\right]\stackrel{\varepsilon\to 0}{\longrightarrow}\exp\left(-\frac{|\boldsymbol{y}|^2}{r_0^2}\right),$$

which shows that there is no refocusing. This is because the TRM elements are too large, and there is no multipathing effect due to the random medium.

In the strongly scattering regime $L\gg\ell_{\rm sca}$ (which is equivalent to $\omega_0^2C(\mathbf{0})L/c_o^2\gg 1$), we find by Proposition 5.4 that

$$\mathbb{E}\left[\hat{u}_{\rm tr}\left(\frac{\boldsymbol{y}}{\varepsilon}+\boldsymbol{x};\frac{\boldsymbol{y}}{\varepsilon}\right)\right]\stackrel{\varepsilon\to 0}{\longrightarrow}\frac{e^{-a_\Omega(L)}r_0^2}{4\pi}\int_{\mathbb{R}^2}\exp\big(-e_\Omega(L)|\boldsymbol{\zeta}|^2-f_\Omega(L)\boldsymbol{x}\cdot\boldsymbol{\zeta}-b_\Omega(L)|\boldsymbol{x}|^2+i\boldsymbol{\zeta}\cdot\boldsymbol{y}\big)d\boldsymbol{\zeta},$$

with

$$\begin{aligned}e_\Omega(z) &= \frac{r_0^2}{4}+d_\Omega(z)-\frac{c_oz}{\omega_0}c_\Omega(z)+\frac{c_o^2z^2}{\omega_0^2}b_\Omega(z)\\ &= \frac{r_0^2}{4}+\frac{Dz^3}{48}\big(\Psi_d-3\Psi_c+3\Psi_b\big)\left(\sqrt{\frac{D\Omega}{4c_o}}z\right),\end{aligned}\tag{6.1}$$

$$\begin{aligned}&f_\Omega(z)c_\Omega(z)-\frac{2c_oz}{\omega_0}b_\Omega(z)\\ &\quad=\frac{\omega_0Dz^2}{16c_o}\big(\Psi_c-2\Psi_b\big)\left(\sqrt{\frac{D\Omega}{4c_o}}z\right).\end{aligned}\tag{6.2}$$

This shows that the mean refocused wave has the form of a Gaussian peak centered at the target location. More exactly, if we consider the case when $\boldsymbol{y}=\mathbf{0}$, then we find that the mean refocused wave is

$$\mathbb{E}\big[\hat{u}_{\mathrm{tr}}(\boldsymbol{x};\mathbf{0})\big] = \frac{e^{-a_\Omega(L)}r_0^2}{4e_\Omega(L)} \exp\big(-g_\Omega(L)|\boldsymbol{x}|^2\big), \tag{6.3}$$

with

$$\begin{aligned} g_\Omega(z) &= b_\Omega(z) - \frac{f_\Omega(z)^2}{4e_\Omega(z)} \\ &= \frac{\omega_0^2 Dz}{16c_o^2}\left(\Psi_b - \frac{\frac{Dz^3}{16}(\Psi_c - 2\Psi_b)^2}{r_0^2 + \frac{Dz^3}{12}(\Psi_d - 3\Psi_c + 3\Psi_b)}\right)\left(\sqrt{\frac{D\Omega}{4c_o}}z\right). \end{aligned} \tag{6.4}$$

When $D\Omega L^2/c_o \ll 1$, we have

$$\mathbb{E}\big[\hat{u}_{\mathrm{tr}}(\boldsymbol{x};\mathbf{0})\big] \simeq \frac{1}{1+\frac{DL^3}{12r_0^2}} \exp\Big(-\frac{\omega_0^2 DL}{16c_o^2}\frac{1+\frac{DL^3}{48r_0^2}}{1+\frac{DL^3}{12r_0^2}}|\boldsymbol{x}|^2\Big), \tag{6.5}$$

which is the expression of the mean refocused wave when $\Omega = 0$ [16], which does not depend on the array element size ρ_0 (which is too large to ensure refocusing) but strongly depends on the properties of the random medium (which is scattering enough to ensure the multipathing effect that gives rise to refocusing). We observe a power-law decay of the mean peak amplitude as a function of the propagation distance.

When $D\Omega L^2/c_o \gg 1$, we have

$$\mathbb{E}\big[\hat{u}_{\mathrm{tr}}(\boldsymbol{x};\mathbf{0})\big] \simeq \frac{2\exp\left(-e^{-i\pi/4}\sqrt{\frac{D\Omega}{4c_o}}L\right)}{1+i\frac{Lc_o}{\Omega r_0^2}} \exp\left(-e^{i\pi/4}\frac{\omega_0^2}{8c_o^2}\sqrt{\frac{Dc_o}{\Omega}}|\boldsymbol{x}|^2\right). \tag{6.6}$$

We observe an exponential decay of the mean peak amplitude, of the form

$$\exp\left(-\sqrt{\frac{D\Omega}{8c_o}}L\right),$$

while the radius of the mean peak becomes equal to

$$\frac{c_o}{\omega_0}2^{7/4}\sqrt[4]{\frac{\Omega}{Dc_o}}.$$

These results (concerning the mean refocused wave) do not depend on the array size r_0 or array element size ρ_0. They show that the amplitude of the mean refocused wave is noticeable provided $D\Omega L^2/(8c_o) < 1$. We will see in the next section that the SNR indeed dramatically decays when this condition is not fulfilled.

6.2. SNR analysis. We now give the general expression of the second-order moment of the refocused field in the scintillation regime.

PROPOSITION 6.2. *In the scintillation regime* (5.6) *the second-order moment of the refocused field is*

$$
\begin{aligned}
&\mathbb{E}\left[\left|\hat{u}_{\rm tr}\left(\frac{\boldsymbol{y}}{\varepsilon}+\boldsymbol{x};\frac{\boldsymbol{y}}{\varepsilon}\right)\right|^2\right] \stackrel{\varepsilon\to 0}{\longrightarrow} \frac{K(L)^2}{(2\pi)^8}\int_{\mathbb{R}^2}\frac{r_0^2}{2\pi}\exp\Big(-\frac{r_0^2|\boldsymbol{\zeta}|^2}{2}+2i\boldsymbol{y}\cdot\boldsymbol{\zeta}\Big)d\boldsymbol{\zeta}\\
&+\frac{2K(L)}{(2\pi)^8}{\rm Re}\iint_{\mathbb{R}^2\times\mathbb{R}^2}\frac{r_0^2}{4\pi}\exp\Big(-\frac{r_0^2|\boldsymbol{\zeta}|^2}{4}+i\boldsymbol{x}\cdot\boldsymbol{\xi}+i\boldsymbol{y}\cdot\boldsymbol{\zeta}-\frac{|\boldsymbol{y}|^2}{r_0^2}\Big)\\
&\quad\times\exp\Big(-i\frac{Lc_o}{\omega_0}\boldsymbol{\xi}\cdot\boldsymbol{\zeta}\Big)A(L,\boldsymbol{\xi},\boldsymbol{\zeta},\Omega)d\boldsymbol{\xi}d\boldsymbol{\zeta}\\
&+\frac{2K(L)}{(2\pi)^8}{\rm Re}\iint_{\mathbb{R}^2\times\mathbb{R}^2}\frac{\rho_0^2r_0^2}{2\pi(\rho_0^2+r_0^2)}\exp\Big(-\frac{r_0^2\rho_0^2|\boldsymbol{\zeta}|^2}{2(r_0^2+\rho_0^2)}+i\frac{2\rho_0^2}{r_0^2+\rho_0^2}\boldsymbol{y}\cdot\boldsymbol{\zeta}-\frac{2|\boldsymbol{y}|^2}{r_0^2+\rho_0^2}\Big)\\
&\quad\times\exp\Big(-i\frac{Lc_o}{\omega_0}\boldsymbol{\xi}\cdot\boldsymbol{\zeta}\Big)A(L,\boldsymbol{\xi},\boldsymbol{\zeta},0)d\boldsymbol{\xi}d\boldsymbol{\zeta}\\
&+\Big|\frac{1}{(2\pi)^4}\iint_{\mathbb{R}^2\times\mathbb{R}^2}\frac{r_0^2}{4\pi}\exp\Big(-\frac{r_0^2|\boldsymbol{\zeta}|^2}{4}+i\boldsymbol{x}\cdot\boldsymbol{\xi}+i\boldsymbol{y}\cdot\boldsymbol{\zeta}-i\frac{Lc_o}{\omega_0}\boldsymbol{\xi}\cdot\boldsymbol{\zeta}\Big)A(L,\boldsymbol{\xi},\boldsymbol{\zeta},\Omega)d\boldsymbol{\xi}d\boldsymbol{\zeta}\Big|^2\\
&+\frac{1}{(2\pi)^8}\iint_{\mathbb{R}^2\times\mathbb{R}^2\times\mathbb{R}^2\times\mathbb{R}^2}\frac{r_0^2\rho_0^2}{(4\pi)^2}\exp\Big(-\frac{r_0^2+\rho_0^2}{8}(|\boldsymbol{\zeta}_a|^2+|\boldsymbol{\zeta}_b|^2)+\frac{r_0^2-\rho_0^2}{4}\boldsymbol{\zeta}_a\cdot\boldsymbol{\zeta}_b\Big)\\
&\quad\times\exp\Big(i\boldsymbol{y}\cdot(\boldsymbol{\zeta}_a-\boldsymbol{\zeta}_b)-i\frac{Lc_o}{\omega_0}(\boldsymbol{\xi}_a\cdot\boldsymbol{\zeta}_a-\boldsymbol{\xi}_b\cdot\boldsymbol{\zeta}_b)\Big)\\
&\quad\times A(L,\boldsymbol{\xi}_a,\boldsymbol{\zeta}_a,0)\overline{A(L,\boldsymbol{\xi}_b,\boldsymbol{\zeta}_b,0)}d\boldsymbol{\xi}_a d\boldsymbol{\xi}_b d\boldsymbol{\zeta}_a d\boldsymbol{\zeta}_b.
\end{aligned}
$$

Proof. The second moment of the refocused wave is given by

$$
\begin{aligned}
\mathbb{E}\left[\left|\hat{u}_{\rm tr}\left(\frac{\boldsymbol{y}}{\varepsilon}+\boldsymbol{x};\frac{\boldsymbol{y}}{\varepsilon}\right)\right|^2\right] &= \mathcal{M}_2\left(\frac{\boldsymbol{y}}{\varepsilon}+\boldsymbol{x},\frac{\boldsymbol{y}}{\varepsilon}+\boldsymbol{x},\frac{\boldsymbol{y}}{\varepsilon}\right)\\
&= M_2^\varepsilon\left(\frac{L}{\varepsilon},\boldsymbol{r}_1=2\frac{\boldsymbol{y}}{\varepsilon}+\boldsymbol{x},\boldsymbol{r}_2=\boldsymbol{0},\boldsymbol{q}_1=\boldsymbol{0},\boldsymbol{q}_2=\boldsymbol{x}\right)\\
&= \frac{1}{(2\pi)^8}\iint\widetilde{M_2^\varepsilon}\left(\frac{L}{\varepsilon},\boldsymbol{\xi}_1,\boldsymbol{\xi}_2,\boldsymbol{\zeta}_1,\boldsymbol{\zeta}_2\right)\\
&\qquad\exp\left(i\boldsymbol{x}\cdot\boldsymbol{\xi}_2+i\left(2\frac{\boldsymbol{y}}{\varepsilon}+\boldsymbol{x}\right)\cdot\boldsymbol{\zeta}_1\right)\\
&\qquad\times\exp\left(-i\frac{Lc_o}{\varepsilon\omega_0}(\boldsymbol{\xi}_1\cdot\boldsymbol{\zeta}_1+\boldsymbol{\xi}_2\cdot\boldsymbol{\zeta}_2)\right)d\boldsymbol{\xi}_1d\boldsymbol{\xi}_2d\boldsymbol{\zeta}_1d\boldsymbol{\zeta}_2,
\end{aligned}
$$

with $\Omega_1=\Omega_2=0$ and $\Omega_3=\Omega$. In the limit $\varepsilon\to 0$, we find from Proposition 5.2 the desired result. ∎

In the weakly scattering regime $L\ll\ell_{\rm sca}$, we find

$$
\begin{aligned}
{\rm Var}\left[\hat{u}_{\rm tr}\left(\frac{\boldsymbol{y}}{\varepsilon}+\boldsymbol{x};\frac{\boldsymbol{y}}{\varepsilon}\right)\right] &= \mathbb{E}\left[\left|\hat{u}_{\rm tr}\left(\frac{\boldsymbol{y}}{\varepsilon}+\boldsymbol{x};\frac{\boldsymbol{y}}{\varepsilon}\right)\right|^2\right]-\left|\mathbb{E}\left[\hat{u}_{\rm tr}\left(\frac{\boldsymbol{y}}{\varepsilon}+\boldsymbol{x};\frac{\boldsymbol{y}}{\varepsilon}\right)\right]\right|^2\\
&\stackrel{\varepsilon\to 0}{\longrightarrow} 0,
\end{aligned}
$$

which follows since the scattering is negligible and the propagation approximately as in a homogeneous medium.

In the strongly scattering regime $L\gg\ell_{\rm sca}$, we find by Proposition 5.4 that

$$
\begin{aligned}
{\rm Var}\left[\hat{u}_{\rm tr}\left(\frac{\boldsymbol{y}}{\varepsilon}+\boldsymbol{x};\frac{\boldsymbol{y}}{\varepsilon}\right)\right] &= \mathbb{E}\left[\left|\hat{u}_{\rm tr}\left(\frac{\boldsymbol{y}}{\varepsilon}+\boldsymbol{x};\frac{\boldsymbol{y}}{\varepsilon}\right)\right|^2\right]-\left|\mathbb{E}\left[\hat{u}_{\rm tr}\left(\frac{\boldsymbol{y}}{\varepsilon}+\boldsymbol{x};\frac{\boldsymbol{y}}{\varepsilon}\right)\right]\right|^2\\
&\stackrel{\varepsilon\to 0}{\longrightarrow}\frac{r_0^2\rho_0^2}{(4\pi)^2}\iint_{\mathbb{R}^2\times\mathbb{R}^2}\exp\left(-\frac{r_0^2+\rho_0^2}{8}(|\boldsymbol{\zeta}_a|^2+|\boldsymbol{\zeta}_b|^2)+\frac{r_0^2-\rho_0^2}{4}\boldsymbol{\zeta}_a\cdot\boldsymbol{\zeta}_b\right)\\
&\qquad\times\exp\big(-d_0(L)(|\boldsymbol{\zeta}_a|^2+|\boldsymbol{\zeta}_b|^2)+i(\boldsymbol{\zeta}_a-\boldsymbol{\zeta}_b)\cdot\boldsymbol{y}\big)d\boldsymbol{\zeta}_a d\boldsymbol{\zeta}_b,
\end{aligned}
$$

with

$$d_0(z) = \frac{Dz^3}{48}.$$

Note that the variance does not depend on the frequency offset Ω, and we recover the result known in the case $\Omega = 0$ [16], while we have shown above that the amplitude of the main refocused wave decays as $|\Omega|$ increases. Therefore the SNR will decrease as $|\Omega|$ increases, as we explain below.

If we consider the case when $\boldsymbol{y} = \mathbf{0}$, then we find that the variance of the refocused wave has the form

$$\mathrm{Var}\big[\hat{u}_{\mathrm{tr}}\big(\boldsymbol{x};\mathbf{0}\big)\big] = \frac{1}{\big(1+\frac{DL^3}{12r_0^2}\big)\big(1+\frac{DL^3}{12\rho_0^2}\big)}. \tag{6.7}$$

The SNR defined by

$$\mathrm{SNR} = \frac{\big|\mathbb{E}\big[\hat{u}_{\mathrm{tr}}\big(\mathbf{0};\mathbf{0}\big)\big]\big|^2}{\mathrm{Var}\big[\hat{u}_{\mathrm{tr}}\big(\boldsymbol{x};\mathbf{0}\big)\big]} \tag{6.8}$$

is given by

$$\mathrm{SNR} = \frac{e^{-2\mathrm{Re}[a_\Omega(L)]}r_0^4}{16|e_\Omega(L)|^2}\left(1+\frac{DL^3}{12r_0^2}\right)\left(1+\frac{DL^3}{12\rho_0^2}\right). \tag{6.9}$$

When $D\Omega L^2/c_o \ll 1$, we have

$$\mathrm{SNR} \simeq \frac{1+\frac{DL^3}{12\rho_0^2}}{1+\frac{DL^3}{12r_0^2}}.$$

This result has already been obtained (when $\Omega = 0$) in [16]. When $DL^3 \gg r_0^2, \rho_0^2$, we find that the SNR varies as r_0^2/ρ_0^2, that is to say, as the number of elements of the TRM.

When $D\Omega L^2/c_o \gg 1$, we have

$$\mathrm{SNR} \simeq \frac{2\exp\left(-\sqrt{\frac{D\Omega}{2c_o}}L\right)}{1+\frac{L^2c_o^2}{\Omega^2 r_0^4}}\left(1+\frac{DL^3}{12r_0^2}\right)\left(1+\frac{DL^3}{12\rho_0^2}\right),$$

which is dominated by the exponentially decaying term.

Conclusion. To summarize, refocusing can be achieved provided $D\Omega L^2/(8c_o) < 1$, which is a condition that depends only on the frequency offset Ω, the coefficient D or paraxial distance $\ell_{\mathrm{par}} = 3/D$, and the propagation distance L.

6.3. The scintillation regime revisited. In the scintillation regime (5.51), where ρ_0 is of the same order as the correlation length of the random medium, we find from Proposition 5.5 that the mean refocused wave is

$$\mathbb{E}\left[\hat{u}_{\mathrm{tr}}\left(\frac{\boldsymbol{y}}{\varepsilon}+\boldsymbol{x};\frac{\boldsymbol{y}}{\varepsilon}\right)\right] \overset{\varepsilon\to 0}{\longrightarrow} \frac{1}{(2\pi)^4} \times \iint_{\mathbb{R}^2\times\mathbb{R}^2} \frac{r_0^2}{4\pi}\exp\Big(-\frac{r_0^2|\boldsymbol{\zeta}|^2}{4} + i\boldsymbol{x}\cdot\boldsymbol{\xi} + i\boldsymbol{y}\cdot\boldsymbol{\zeta} - i\frac{Lc_o}{\omega_0}\boldsymbol{\xi}\cdot\boldsymbol{\zeta}\Big)A(L,\boldsymbol{\xi},\boldsymbol{\zeta},\Omega)d\boldsymbol{\xi}d\boldsymbol{\zeta},$$

where A is given by (5.52).

In the weakly scattering regime $L \ll \ell_{\rm sca}$ (which is equivalent to $\omega_0^2 C(\mathbf{0})L/c_o^2 \ll 1$), we have $A(L,\boldsymbol{\xi},\boldsymbol{\zeta},\Omega) = (2\pi)^4 \phi^1_{\sqrt{2}\rho_0}(\boldsymbol{\xi}) \exp(ic_o\Omega|\boldsymbol{\xi}|^2 L/\omega_0^2)$ and therefore

$$\mathbb{E}\left[\hat{u}_{\rm tr}\left(\frac{\boldsymbol{y}}{\varepsilon}+\boldsymbol{x};\frac{\boldsymbol{y}}{\varepsilon}\right)\right] \stackrel{\varepsilon\to 0}{\longrightarrow} \iint_{\mathbb{R}^2\times\mathbb{R}^2} \frac{\rho_0^2 r_0^2}{4\pi^2} \exp\left(-\frac{r_0^2|\boldsymbol{\zeta}|^2}{4} - \rho_0^2|\boldsymbol{\xi}|^2 + i\boldsymbol{x}\cdot\boldsymbol{\xi} + i\boldsymbol{y}\cdot\boldsymbol{\zeta} + i\frac{c_o\Omega L}{\omega_0^2}|\boldsymbol{\xi}|^2 - i\frac{Lc_o}{\omega_0}\boldsymbol{\xi}\cdot\boldsymbol{\zeta}\right) d\boldsymbol{\xi}d\boldsymbol{\zeta}.$$

If $\boldsymbol{y}=\mathbf{0}$, then we get

$$\mathbb{E}\big[\hat{u}_{\rm tr}(\boldsymbol{x};\mathbf{0})\big] \stackrel{\varepsilon\to 0}{\longrightarrow} \frac{1}{1+\frac{c_o^2L^2}{\omega_0^2\rho_0^2r_0^2} - i\frac{c_o\Omega L}{\omega_0^2\rho_0^2}} \exp\left(-\frac{|\boldsymbol{x}|^2}{4\rho_0^2\big(1+\frac{c_o^2L^2}{\omega_0^2\rho_0^2r_0^2} - i\frac{c_o\Omega L}{\omega_0^2\rho_0^2}\big)}\right),$$

which shows that we can get refocusing because the TRM element size is small enough. The frequency shift $|\Omega|$ should be smaller than $\omega_0^2\rho_0^2/(c_oL)$ so that the quality of the refocusing is not affected.

In the strongly scattering regime $L \gg \ell_{\rm sca}$ (which is equivalent to $\omega_0^2 C(\mathbf{0})L/c_o^2 \gg 1$), we find by Proposition 5.7 that

$$\mathbb{E}\left[\hat{u}_{\rm tr}\left(\frac{\boldsymbol{y}}{\varepsilon}+\boldsymbol{x};\frac{\boldsymbol{y}}{\varepsilon}\right)\right] = \frac{e^{-a_\Omega(L)}r_0^2}{4\pi}\int \exp\big(-e_\Omega(L)|\boldsymbol{\zeta}|^2 - f_\Omega(L)\boldsymbol{x}\cdot\boldsymbol{\zeta} - b_\Omega(L)|\boldsymbol{x}|^2 + i\boldsymbol{\zeta}\cdot\boldsymbol{y}\big)d\boldsymbol{\zeta},$$

with a_Ω defined by (5.39), (e_Ω, f_Ω) defined by (6.1)–(6.2), and $(\Psi_a,\Psi_b,\Psi_c,\Psi_d)$ defined by (5.57)–(5.60). More exactly, if we consider the case when $\boldsymbol{y}=\mathbf{0}$, then we find that the mean refocused wave is

$$\mathbb{E}\big[\hat{u}_{\rm tr}(\boldsymbol{x};\mathbf{0})\big] = \frac{e^{-a_\Omega(L)}r_0^2}{4e_\Omega(L)} \exp\big(-g_\Omega(L)|\boldsymbol{x}|^2\big), \tag{6.10}$$

with g_Ω defined by (6.4).

When $D\Omega L^2/c_o \ll 1$, we have

$$\mathbb{E}\big[\hat{u}_{\rm tr}(\boldsymbol{x};\mathbf{0})\big] \simeq \frac{1}{1+\frac{DL^3}{12r_0^2}+\frac{c_o^2L^2}{\omega_0^2\rho_0^2r_0^2}} \exp\Big(-\frac{\frac{\omega_0^2DL}{16c_o^2}\big(1+\frac{DL^3}{48r_0^2}\big)+\frac{1}{4\rho_0^2}\big(1+\frac{DL^3}{12r_0^2}\big)}{1+\frac{DL^3}{12r_0^2}+\frac{c_o^2L^2}{\omega_0^2\rho_0^2r_0^2}}|\boldsymbol{x}|^2\Big). \tag{6.11}$$

We can identify the radius R of the mean refocused wave:

$$R^2 = \frac{1+\frac{DL^3}{12r_0^2}+\frac{c_o^2L^2}{\omega_0^2\rho_0^2r_0^2}}{\frac{\omega_0^2DL}{8c_o^2}\big(1+\frac{DL^3}{48r_0^2}\big)+\frac{1}{2\rho_0^2}\big(1+\frac{DL^3}{12r_0^2}\big)}. \tag{6.12}$$

The radius of the mean refocused wave is smaller when ρ_0 is smaller and when the random medium is more scattering (i.e., D is larger). When ρ_0 becomes large, we recover the expression (6.5).

When $D\Omega L^2/c_o \gg 1$, we get the result (6.6), and we observe again an exponential decay of the mean peak amplitude.

Finally, we find from Proposition 5.6 that

$$\lim_{\varepsilon\to 0}\mathbb{E}\left[\left|\hat{u}_{\rm tr}\left(\frac{\boldsymbol{y}}{\varepsilon}+\boldsymbol{x};\frac{\boldsymbol{y}}{\varepsilon}\right)\right|^2\right] = \lim_{\varepsilon\to 0}\left|\mathbb{E}\left[\hat{u}_{\rm tr}\left(\frac{\boldsymbol{y}}{\varepsilon}+\boldsymbol{x};\frac{\boldsymbol{y}}{\varepsilon}\right)\right]\right|^2. \tag{6.13}$$

The refocused wave is statistically stable in this regime, because there are many elements (of the order of ε^{-2}) in the TRM.

7. Time-reversal stability. We address the situation described in section 3.2 in the scintillation regime (5.6). We consider a pulse whose bandwidth is small, of order ε:

$$\hat{f}^{\varepsilon}(\omega) = \frac{\sqrt{2\pi}}{\varepsilon B} \exp\Big(- \frac{(\omega-\omega_0)^2}{2\varepsilon^2 B^2}\Big).$$

The goal is to determine the profile of the refocused wave and its SNR. In particular we want to determine for which bandwidth B time-reversal refocusing is statistically stable.

7.1. The mean refocused wave. In the limit $\varepsilon \to 0$, we find from (3.9) and Proposition 5.1 that the mean refocused wave is given by

$$\begin{aligned}
&\mathbb{E}\left[u_{\rm tr}\left(\frac{t}{\varepsilon}, \frac{\boldsymbol{y}}{\varepsilon} + \boldsymbol{x}; \frac{\boldsymbol{y}}{\varepsilon}\right)\right] \\
&\stackrel{\varepsilon\to 0}{\longrightarrow} \frac{\exp(-B^2t^2/2)e^{-i\omega_0 t/\varepsilon}}{(2\pi)^4}\Big\{K(L)\exp\Big(-\frac{|\boldsymbol{y}|^2}{r_0^2}\Big) \\
&+ \iint_{\mathbb{R}^2\times\mathbb{R}^2} \frac{r_0^2}{4\pi}\exp\Big(-\frac{r_0^2|\boldsymbol{\zeta}|^2}{4} + i\boldsymbol{x}\cdot\boldsymbol{\xi} + i\boldsymbol{y}\cdot\boldsymbol{\zeta} - i\frac{Lc_o}{\omega_0}\boldsymbol{\xi}\cdot\boldsymbol{\zeta}\Big)A(L,\boldsymbol{\xi},\boldsymbol{\zeta},0)d\boldsymbol{\xi}d\boldsymbol{\zeta}\Big\}.
\end{aligned}$$

In the weakly scattering regime $L \ll \ell_{\rm sca}$, we find

$$\mathbb{E}\left[u_{\rm tr}\left(\frac{t}{\varepsilon}, \frac{\boldsymbol{y}}{\varepsilon} + \boldsymbol{x}; \frac{\boldsymbol{y}}{\varepsilon}\right)\right] = \exp(-B^2t^2/2)e^{-i\omega_0 t/\varepsilon}\exp\Big(-\frac{|\boldsymbol{y}|^2}{r_0^2}\Big),$$

which shows that there is not refocusing.

In the strongly scattering regime $L \gg \ell_{\rm sca}$, we find by Proposition 5.4 that

$$\begin{aligned}
\mathbb{E}\left[u_{\rm tr}\left(\frac{t}{\varepsilon}, \frac{\boldsymbol{y}}{\varepsilon} + \boldsymbol{x}; \frac{\boldsymbol{y}}{\varepsilon}\right)\right] &= \frac{r_0^2\exp(-B^2t^2/2)e^{-i\omega_0 t/\varepsilon}}{4\pi} \\
&\times \int_{\mathbb{R}^2} \exp\big(-e_0(L)|\boldsymbol{\zeta}|^2 - f_0(L)\boldsymbol{x}\cdot\boldsymbol{\zeta} - b_0(L)|\boldsymbol{x}|^2 + i\boldsymbol{\zeta}\cdot\boldsymbol{y}\big)d\boldsymbol{\zeta},
\end{aligned}$$

with

$$b_0(z) = \frac{\omega_0^2 Dz}{16c_o^2}, \qquad e_0(z) = \frac{r_0^2}{4} + \frac{Dz^3}{48}, \qquad f_0(z) = -\frac{\omega_0 Dz^2}{16c_o}.$$

In particular, if $\boldsymbol{y} = \boldsymbol{0}$, we find

$$\mathbb{E}\left[u_{\rm tr}\left(\frac{t}{\varepsilon}, \boldsymbol{x}; \boldsymbol{0}\right)\right] = \frac{e^{-i\omega_0 t/\varepsilon}}{1+\frac{DL^3}{12r_0^2}}\exp\left(-\frac{B^2t^2}{2} - \frac{\omega_0^2 DL}{16c_o^2}\frac{1+\frac{DL^3}{48r_0^2}}{1+\frac{DL^3}{12r_0^2}}|\boldsymbol{x}|^2\right), \tag{7.1}$$

which shows that there is refocusing, with a focal spot radius that is all the smaller as the medium is more scattering.

7.2. SNR analysis. Let us consider the second moment of the refocused wave. In the limit $\varepsilon \to 0$, we find from Proposition 5.2 that

$$
\begin{aligned}
&\mathbb{E}\left[\left|u_{\rm tr}\left(\frac{t}{\varepsilon},\frac{\boldsymbol{y}}{\varepsilon}+\boldsymbol{x};\frac{\boldsymbol{y}}{\varepsilon}\right)\right|^2\right]\\
&\quad\stackrel{\varepsilon\to 0}{\longrightarrow}\frac{K(L)^2\exp(-B^2t^2)}{(2\pi)^8}\int_{\mathbb{R}^2}\frac{r_0^2}{2\pi}\exp\Big(-\frac{r_0^2|\boldsymbol{\zeta}|^2}{2}+2i\boldsymbol{y}\cdot\boldsymbol{\zeta}\Big)d\boldsymbol{\zeta}\\
&\quad+\frac{2K(L)\exp(-B^2t^2)}{(2\pi)^8}{\rm Re}\int_{\mathbb{R}}\iint_{\mathbb{R}^2\times\mathbb{R}^2}\frac{r_0^2}{4\pi}\exp\Big(-\frac{r_0^2|\boldsymbol{\zeta}|^2}{4}+i\boldsymbol{x}\cdot\boldsymbol{\xi}+i\boldsymbol{y}\cdot\boldsymbol{\zeta}-\frac{|\boldsymbol{y}|^2}{r_0^2}\Big)\\
&\qquad\times\exp\Big(-i\frac{Lc_o}{\omega_0}\boldsymbol{\xi}\cdot\boldsymbol{\zeta}\Big)A(L,\boldsymbol{\xi},\boldsymbol{\zeta},0)d\boldsymbol{\xi}d\boldsymbol{\zeta}d\Omega\\
&\quad+\frac{2K(L)}{(2\pi)^8\sqrt{\pi}B}{\rm Re}\int_{\mathbb{R}}\iint_{\mathbb{R}^2\times\mathbb{R}^2}\frac{\rho_0^2r_0^2}{2\pi(\rho_0^2+r_0^2)}\\
&\qquad\times\exp\Big(-\frac{r_0^2\rho_0^2|\boldsymbol{\zeta}|^2}{2(r_0^2+\rho_0^2)}+i\frac{2\rho_0^2}{r_0^2+\rho_0^2}\boldsymbol{y}\cdot\boldsymbol{\zeta}-\frac{2|\boldsymbol{y}|^2}{r_0^2+\rho_0^2}\Big)\\
&\qquad\times\exp\Big(-i\frac{Lc_o}{\omega_0}\boldsymbol{\xi}\cdot\boldsymbol{\zeta}-2i\Omega t-\frac{\Omega^2}{B^2}\Big)A(L,\boldsymbol{\xi},\boldsymbol{\zeta},\Omega)d\boldsymbol{\xi}d\boldsymbol{\zeta}d\Omega\\
&\quad+\Big|\frac{\exp(-B^2t^2/2)}{(2\pi)^4}\iint_{\mathbb{R}^2\times\mathbb{R}^2}\frac{r_0^2}{4\pi}\\
&\qquad\times\exp\Big(-\frac{r_0^2|\boldsymbol{\zeta}|^2}{4}+i\boldsymbol{x}\cdot\boldsymbol{\xi}+i\boldsymbol{y}\cdot\boldsymbol{\zeta}-i\frac{Lc_o}{\omega_0}\boldsymbol{\xi}\cdot\boldsymbol{\zeta}\Big)A(L,\boldsymbol{\xi},\boldsymbol{\zeta},0)d\boldsymbol{\xi}d\boldsymbol{\zeta}\Big|^2\\
&\quad+\frac{1}{(2\pi)^8\sqrt{\pi}B}\int_{\mathbb{R}}\iint_{\mathbb{R}^2\times\mathbb{R}^2\times\mathbb{R}^2\times\mathbb{R}^2}\frac{r_0^2\rho_0^2}{(4\pi)^2}\\
&\qquad\times\exp\Big(-\frac{r_0^2+\rho_0^2}{8}(|\boldsymbol{\zeta}_a|^2+|\boldsymbol{\zeta}_b|^2)+\frac{r_0^2-\rho_0^2}{4}\boldsymbol{\zeta}_a\cdot\boldsymbol{\zeta}_b\Big)\\
&\qquad\times\exp\Big(i\boldsymbol{y}\cdot(\boldsymbol{\zeta}_a-\boldsymbol{\zeta}_b)-i\frac{Lc_o}{\omega_0}(\boldsymbol{\xi}_a\cdot\boldsymbol{\zeta}_a-\boldsymbol{\xi}_b\cdot\boldsymbol{\zeta}_b)\Big)A(L,\boldsymbol{\xi}_a,\boldsymbol{\zeta}_a,\Omega)\overline{A(L,\boldsymbol{\xi}_b,\boldsymbol{\zeta}_b,\Omega)}\\
&\qquad\times\exp\Big(-2i\Omega t-\frac{\Omega^2}{B^2}\Big)d\boldsymbol{\xi}_a d\boldsymbol{\xi}_b d\boldsymbol{\zeta}_a d\boldsymbol{\zeta}_b d\Omega.
\end{aligned}
$$

In the weakly scattering regime $L\ll\ell_{\rm sca}$, we get

$$
{\rm Var}\left[u_{\rm tr}\left(\frac{t}{\varepsilon},\frac{\boldsymbol{y}}{\varepsilon}+\boldsymbol{x};\frac{\boldsymbol{y}}{\varepsilon}\right)\right]=\mathbb{E}\left[\left|u_{\rm tr}\left(\frac{t}{\varepsilon},\frac{\boldsymbol{y}}{\varepsilon}+\boldsymbol{x};\frac{\boldsymbol{y}}{\varepsilon}\right)\right|^2\right]-\left|\mathbb{E}\left[u_{\rm tr}\left(\frac{t}{\varepsilon},\frac{\boldsymbol{y}}{\varepsilon}+\boldsymbol{x};\frac{\boldsymbol{y}}{\varepsilon}\right)\right]\right|^2
\stackrel{\varepsilon\to 0}{\longrightarrow}0.
$$

In the strongly scattering regime $L\gg\ell_{\rm sca}$, we find by Proposition 5.4 that

$$
\begin{aligned}
&{\rm Var}\left[u_{\rm tr}\left(\frac{t}{\varepsilon},\frac{\boldsymbol{y}}{\varepsilon}+\boldsymbol{x};\frac{\boldsymbol{y}}{\varepsilon}\right)\right]=\mathbb{E}\left[\left|u_{\rm tr}\left(\frac{t}{\varepsilon},\frac{\boldsymbol{y}}{\varepsilon}+\boldsymbol{x};\frac{\boldsymbol{y}}{\varepsilon}\right)\right|^2\right]-\left|\mathbb{E}\left[u_{\rm tr}\left(\frac{t}{\varepsilon},\frac{\boldsymbol{y}}{\varepsilon}+\boldsymbol{x};\frac{\boldsymbol{y}}{\varepsilon}\right)\right]\right|^2\\
&\stackrel{\varepsilon\to 0}{\longrightarrow}\frac{r_0^2\rho_0^2}{(4\pi)^2B\sqrt{\pi}}\int_{\mathbb{R}}\iint_{\mathbb{R}^2\times\mathbb{R}^2}\exp\Big(-\frac{r_0^2+\rho_0^2}{8}(|\boldsymbol{\zeta}_a|^2+|\boldsymbol{\zeta}_b|^2)+\frac{r_0^2-\rho_0^2}{4}\boldsymbol{\zeta}_a\cdot\boldsymbol{\zeta}_b\Big)\\
&\quad\times\exp\big(-a_\Omega(L)-h_\Omega(L)|\boldsymbol{\zeta}_a|^2-\overline{a_\Omega}(L)-\overline{h_\Omega}(L)|\boldsymbol{\zeta}_b|^2\big)\\
&\quad\times\exp\Big(i(\boldsymbol{\zeta}_a-\boldsymbol{\zeta}_b)\cdot\boldsymbol{y}-2i\Omega t-\frac{\Omega^2}{B^2}\Big)d\boldsymbol{\zeta}_a d\boldsymbol{\zeta}_b d\Omega,
\end{aligned}
$$

with

$$h_\Omega(z) = \frac{c_o^2 z^2}{\omega_0^2} b_\Omega(z) - \frac{c_o z}{\omega_0} c_\Omega(z) + d_\Omega(z)$$
$$= \frac{Dz^3}{48}\big(\Psi_d - 3\Psi_c + 3\Psi_b\big)\left(\sqrt{\frac{D\Omega}{4c_o}}z\right). \tag{7.2}$$

For $\boldsymbol{y} = \mathbf{0}$, this gives

$$\mathrm{Var}\left[u_{\mathrm{tr}}\left(\frac{t}{\varepsilon}, \boldsymbol{x}; \mathbf{0}\right)\right] = \frac{1}{\sqrt{\pi}}\int_{\mathbb{R}} \hat{a}_s \exp\big(-s^2 - 2iBts\big)\Big(1 + \frac{DL^3\hat{h}_s}{12\rho_0^2}\Big)^{-1}$$
$$\times \Big(1 + \frac{DL^3\hat{h}_s}{12r_0^2}\Big)^{-1} ds,$$

with $\hat{a}_s = \exp(-2\mathrm{Re}(a_{Bs}(L)))$ and $\frac{DL^3}{12}\hat{h}_s = 4\mathrm{Re}(h_{Bs}(L))$. More explicitly,

$$\hat{a}_s = \hat{\mathcal{A}}\left(\frac{DBL^2|s|}{4c_o}\right), \qquad \hat{\mathcal{A}}(s) = \frac{2}{\big(\cos + \cosh\big)\big(\sqrt{2s}\big)},$$
$$\hat{h}_s = \hat{\mathcal{H}}\left(\frac{DBL^2|s|}{4c_o}\right), \qquad \hat{\mathcal{H}}(s) = \mathrm{Re}\Big\{\big(\Psi_d - 3\Psi_c + 3\Psi_b\big)\big(\sqrt{s}\big)\Big\}.$$

The SNR defined by

$$\mathrm{SNR} = \frac{\big|\mathbb{E}[u_{\mathrm{tr}}\big(0, \mathbf{0}; \mathbf{0}\big)]\big|^2}{\mathrm{Var}\big[u_{\mathrm{tr}}\big(0, \boldsymbol{x}; \mathbf{0}\big)\big]}$$

is therefore

$$\mathrm{SNR}^{-1} = \frac{2}{\sqrt{\pi}}\int_0^\infty \hat{\mathcal{A}}\left(\frac{DBL^2 s}{4c_o}\right)\frac{\big(1 + \frac{DL^3}{12r_0^2}\big)^2 \exp\big(-s^2\big)}{\big(1 + \frac{DL^3}{12\rho_0^2}\hat{\mathcal{H}}\big(\frac{DBL^2 s}{4c_o}\big)\big)\big(1 + \frac{DL^3}{12r_0^2}\hat{\mathcal{H}}\big(\frac{DBL^2 s}{4c_o}\big)\big)} ds. \tag{7.3}$$

We can observe that there is a complicated interplay between spatial and frequency effects that depends on three dimensionless parameters: $\frac{DL^3}{12r_0^2}$, $\frac{DL^3}{12\rho_0^2}$, and $\frac{DBL^2}{4c_o}$. We plot in Figure 7.1 the SNR for different values of these three parameters, where we can see that the SNR increases with these three parameters, and analyze below its asymptotic behavior.

The functions $\hat{\mathcal{A}}$ and $\hat{\mathcal{H}}$ satisfy

$$\hat{\mathcal{A}}(s) \simeq \begin{cases} 1 & \text{if } s \ll 1, \\ 4\exp\big(-\sqrt{2s}\big) & \text{if } s \gg 1, \end{cases} \qquad \hat{\mathcal{H}}(s) \simeq \begin{cases} 1 & \text{if } s \ll 1, \\ \frac{3}{4\sqrt{2}}s^{-3/2} & \text{if } s \gg 1. \end{cases}$$

Therefore, if B is much smaller than $4c_o/(DL^2)$, then

$$\mathrm{SNR} \simeq \frac{1 + \frac{DL^3}{12\rho_0^2}}{1 + \frac{DL^3}{12r_0^2}}, \tag{7.4}$$

which shows that the source bandwidth does not affect the statistical stability of the refocused wave under these conditions. We have

$$\mathrm{SNR} \simeq \begin{cases} 1 & \text{if } \rho_0^2 > \dfrac{DL^3}{12}, \\ \dfrac{DL^3}{12\rho_0^2} & \text{if } r_0^2 > \dfrac{DL^3}{12} > \rho_0^2, \\ \dfrac{r_0^2}{\rho_0^2} & \text{if } \dfrac{DL^3}{12} > r_0^2. \end{cases} \tag{7.5}$$

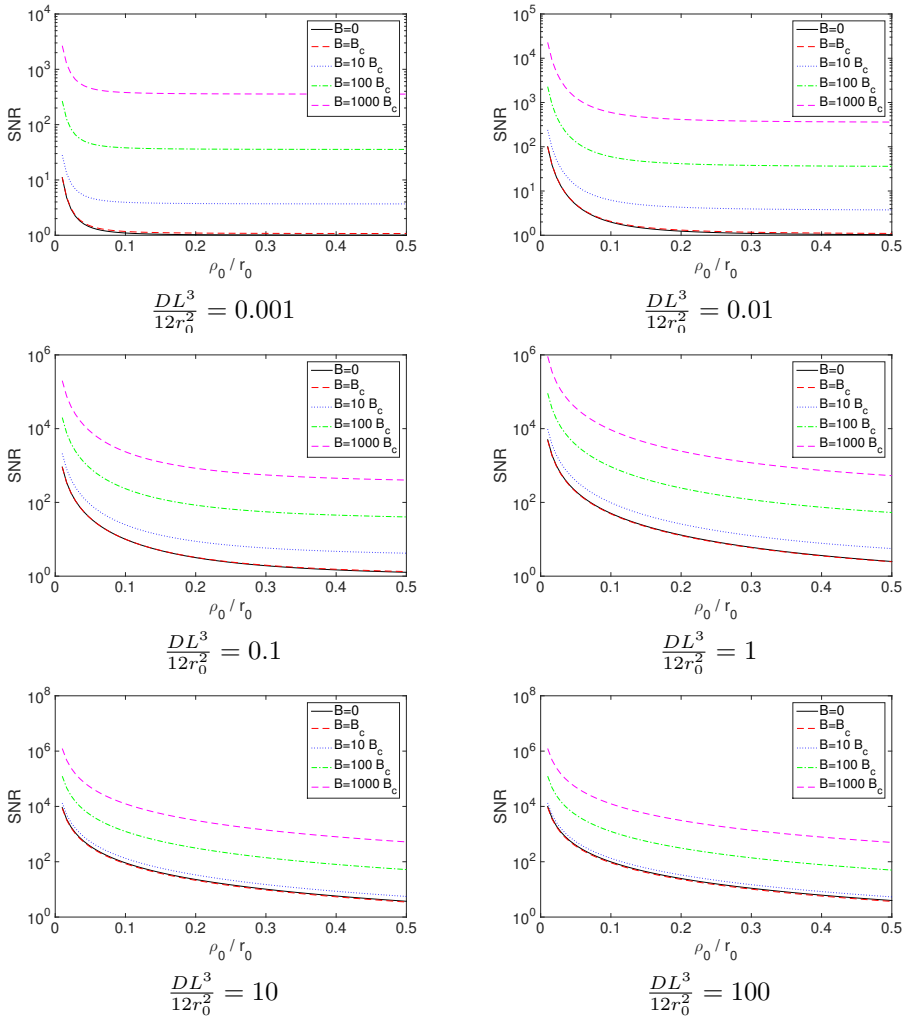

FIG. 7.1. *SNR (7.3) of the time-reversed refocused wave. We denote* $B_c = \frac{4c_o}{DL^2}$. *The value of the SNR for* $B = 0$ *is (7.4).*

In particular, we recover the fact that, when $DL^3/12 \gg r_0^2$, the SNR is equal to the number r_0^2/ρ_0^2 of elements of the TRM.

If B is much larger than $4c_o/(DL^2)$, then

$$\text{SNR}^{-1} \simeq \frac{4c_o}{DBL^2}\frac{2}{\sqrt{\pi}}\int_0^\infty \hat{\mathcal{A}}(s)\frac{\left(1+\frac{DL^3}{12r_0^2}\right)^2}{\left(1+\frac{DL^3}{12\rho_0^2}\hat{\mathcal{H}}(s)\right)\left(1+\frac{DL^3}{12r_0^2}\hat{\mathcal{H}}(s)\right)}ds, \tag{7.6}$$

and we find

$$\text{SNR} \simeq \begin{cases} \dfrac{DL^2B}{4c_o\mathcal{A}_1} & \text{if } \rho_0^2 > \dfrac{DL^3}{12}, \\ \dfrac{DL^2B}{4c_o\mathcal{A}_2}\dfrac{DL^3}{12\rho_0^2} & \text{if } r_0^2 > \dfrac{DL^3}{12} > \rho_0^2, \\ \dfrac{DL^2B}{4c_o\mathcal{A}_3}\dfrac{r_0^2}{\rho_0^2} & \text{if } \dfrac{DL^3}{12} > r_0^2, \end{cases} \tag{7.7}$$

where

$$\mathcal{A}_j = \frac{2}{\sqrt{\pi}} \int_0^\infty \frac{\hat{\mathcal{A}}(s)}{\hat{\mathcal{H}}(s)^{j-1}} ds,$$

or more explicitly $\mathcal{A}_1 \simeq 2.81$, $\mathcal{A}_2 \simeq 4.40$, and $\mathcal{A}_3 \simeq 8.05$. This shows that the source bandwidth improves the statistical stability of the refocused wave, provided it is larger than $4c_o/(DL^2)$. In particular, if scattering is so strong that both $DL^3/12 \gg r_0^2$ and $4c_o/(DL^2) \ll B$, then the SNR is proportional to the number of elements r_0^2/ρ_0^2 of the TRM times the number of uncorrelated frequency components $(DBL^2)/(4c_o)$ (i.e., the ratio of B over the coherence frequency $4c_o/(DL^2)$). The equations (7.5) and (7.7) give the SNR in the different cases and quantify the usual assertion found in the literature that the profile of the time-reversed field is self-averaging by independence of the frequency components of the wave field.

7.3. The scintillation regime revisited. In the scintillation regime (5.51) (in which ρ_0 is of the same order as the correlation length of the random medium), we find from Proposition 5.5 that the mean refocused field is

$$\mathbb{E}\left[u_{\rm tr}\left(\frac{t}{\varepsilon}, \frac{\boldsymbol{y}}{\varepsilon} + \boldsymbol{x}; \frac{\boldsymbol{y}}{\varepsilon}\right)\right] \stackrel{\varepsilon\to 0}{\longrightarrow} \frac{\exp(-B^2t^2/2)e^{-i\omega_0 t/\varepsilon}}{(2\pi)^4}$$
$$\times \iint_{\mathbb{R}^2\times\mathbb{R}^2} \frac{r_0^2}{4\pi} \exp\Big(-\frac{r_0^2|\boldsymbol{\zeta}|^2}{4} + i\boldsymbol{x}\cdot\boldsymbol{\xi} + i\boldsymbol{y}\cdot\boldsymbol{\zeta} - i\frac{Lc_o}{\omega_0}\boldsymbol{\xi}\cdot\boldsymbol{\zeta}\Big) A(L,\boldsymbol{\xi},\boldsymbol{\zeta},0) d\boldsymbol{\xi} d\boldsymbol{\zeta},$$

where A is given by (5.52).

In the weakly scattering regime $L \ll \ell_{\rm sca}$, we find

$$\mathbb{E}\left[u_{\rm tr}\left(\frac{t}{\varepsilon}, \frac{\boldsymbol{y}}{\varepsilon} + \boldsymbol{x}; \frac{\boldsymbol{y}}{\varepsilon}\right)\right] \stackrel{\varepsilon\to 0}{\longrightarrow} \exp(-B^2t^2/2)e^{-i\omega_0 t/\varepsilon}$$
$$\times \iint_{\mathbb{R}^2\times\mathbb{R}^2} \frac{\rho_0^2 r_0^2}{4\pi^2} \exp\Big(-\frac{r_0^2|\boldsymbol{\zeta}|^2}{4} - \rho_0^2|\boldsymbol{\xi}|^2 + i\boldsymbol{x}\cdot\boldsymbol{\xi} + i\boldsymbol{y}\cdot\boldsymbol{\zeta} - i\frac{Lc_o}{\omega_0}\boldsymbol{\xi}\cdot\boldsymbol{\zeta}\Big) d\boldsymbol{\xi} d\boldsymbol{\zeta}.$$

More exactly, if $\boldsymbol{y} = \boldsymbol{0}$, we get

$$\mathbb{E}\left[u_{\rm tr}\left(\frac{t}{\varepsilon}, \boldsymbol{x}; \boldsymbol{0}\right)\right] \stackrel{\varepsilon\to 0}{\longrightarrow} \frac{\exp(-B^2t^2/2)e^{-i\omega_0 t/\varepsilon}}{1 + \frac{c_o^2L^2}{\omega_0^2\rho_0^2r_0^2}} \exp\left(-\frac{|\boldsymbol{x}|^2}{4\rho_0^2\big(1 + \frac{c_o^2L^2}{\omega_0^2\rho_0^2r_0^2}\big)}\right),$$

which shows that we get refocusing because the TRM element size ρ_0 is small enough. When ρ_0 becomes very small, i.e., smaller than $c_oL/(\omega_0 r_0)$, then the radius of the refocused wave is $\sqrt{2}c_oL/(\omega_0 r_0)$, which is the diffraction limit or Rayleigh resolution formula.

In the strongly scattering regime $L \gg \ell_{\rm sca}$, we find by Proposition 5.7 that

$$\mathbb{E}\left[u_{\rm tr}\left(\frac{t}{\varepsilon}, \frac{\boldsymbol{y}}{\varepsilon} + \boldsymbol{x}; \frac{\boldsymbol{y}}{\varepsilon}\right)\right] = \frac{r_0^2 \exp(-B^2t^2/2)e^{-i\omega_0 t/\varepsilon}}{4\pi}$$
$$\times \int_{\mathbb{R}^2} \exp\big(-e_0(L)|\boldsymbol{\zeta}|^2 - f_0(L)\boldsymbol{x}\cdot\boldsymbol{\zeta} - b_0(L)|\boldsymbol{x}|^2 + i\boldsymbol{\zeta}\cdot\boldsymbol{y}\big) d\boldsymbol{\zeta},$$

with

$$b_0(z) = \frac{\omega_0^2 Dz}{16c_o^2} + \frac{1}{4\rho_0^2}, \qquad e_0(z) = \frac{r_0^2}{4} + \frac{Dz^3}{48} + \frac{c_o^2z^2}{4\omega_0^2\rho_0^2}, \qquad f_0(z) = -\frac{\omega_0 Dz^2}{16c_o} - \frac{c_oz}{2\omega_0\rho_0^2}.$$

In particular, if $\boldsymbol{y} = \mathbf{0}$, we find

$$\mathbb{E}\left[u_{\rm tr}\left(\frac{t}{\varepsilon},\boldsymbol{x};\mathbf{0}\right)\right] = \frac{e^{-i\omega_0 t/\varepsilon}}{1+\frac{DL^3}{12r_0^2}+\frac{c_o^2L^2}{\omega_0^2\rho_0^2r_0^2}}\exp\Big(-\frac{B^2t^2}{2}\Big) \times \exp\left(-\frac{\frac{\omega_0^2DL}{16c_o^2}\big(1+\frac{DL^3}{48r_0^2}\big)+\frac{1}{4\rho_0^2}\big(1+\frac{DL^3}{12r_0^2}\big)}{1+\frac{DL^3}{12r_0^2}+\frac{c_o^2L^2}{\omega_0^2\rho_0^2r_0^2}}|\boldsymbol{x}|^2\right), \tag{7.8}$$

which makes it possible to identify the amplitude and the radius R of the refocused wave (as in (6.11)–(6.12)):

$$R^2 = \frac{1+\frac{DL^3}{12r_0^2}+\frac{c_o^2L^2}{\omega_0^2\rho_0^2r_0^2}}{\frac{\omega_0^2DL}{8c_o^2}\big(1+\frac{DL^3}{48r_0^2}\big)+\frac{1}{2\rho_0^2}\big(1+\frac{DL^3}{12r_0^2}\big)}. \tag{7.9}$$

The radius is smaller when the TRM element size ρ_0 is smaller (we have $\partial R/\partial\rho_0 > 0$) and when the random medium is more scattering (we have $\partial R/\partial D < 0$). It is not surprising that time-reversal refocusing is improved when the TRM has many array elements and better resolve the wave field on the mirror; moreover, it is well-known that random scattering improves time-reversal refocusing by multipathing [3, 9]. When ρ_0 becomes very small, i.e., smaller than $c_oL/(\omega_0 r_0)$ and $c_o/(\omega_0 DL)$, then the radius of the refocused wave is equal to

$$R = \frac{\sqrt{2}c_oL}{\omega_0\sqrt{r_0^2+\frac{DL^3}{12}}},$$

which is the Rayleigh resolution formula but with the enhanced TRM radius $r_{\rm eff} = \sqrt{r_0^2+\frac{DL^3}{12}}$. This result can be found in the literature [3].

Finally, we find from Proposition 5.6 that

$$\lim_{\varepsilon\to 0}\mathbb{E}\left[\left|u_{\rm tr}\left(\frac{t}{\varepsilon},\frac{\boldsymbol{y}}{\varepsilon}+\boldsymbol{x};\frac{\boldsymbol{y}}{\varepsilon}\right)\right|^2\right] = \lim_{\varepsilon\to 0}\left|\mathbb{E}\left[u_{\rm tr}\left(\frac{t}{\varepsilon},\frac{\boldsymbol{y}}{\varepsilon}+\boldsymbol{x};\frac{\boldsymbol{y}}{\varepsilon}\right)\right]\right|^2. \tag{7.10}$$

The refocused wave is statistically stable in this regime, because there are many elements (of the order of ε^{-2}) in the TRM.

8. Conclusion. In this paper we have analyzed the fourth-order moment of the random paraxial Green's function at four different frequencies. We have obtained a complete characterization in the scintillation regime, which makes it possible to quantify the speckle memory effect in the frequency domain in terms of the propagation distance through the scattering medium and statistics of the medium fluctuations. Using this result we have also been able to obtain for the first time a quantitative characterization of the statistical stability in the classic time-reversal refocusing experiment. This characterization depends on the radius of the time-reversal mirror, the size of its elements, and the source bandwidth, as well as the statistics of the medium fluctuations. As anticipated and observed in experiments [6, 23], when the medium is strongly scattering, the SNR of the time-reversed refocused wave is given by the number of elements of the time-reversal mirror times the number of independent frequency components in the source bandwidth.

The results of the paper are obtained in the white-noise paraxial regime, which holds when the wavelength is smaller than the correlation length of the medium and

the beam radius, which are themselves smaller than the propagation distance. In such a regime backscattering is negligible. Beyond this regime, when backscattering becomes significant, other asymptotic theories could turn out to be more relevant and useful, such as radiative transfer theory. This problem is left for future research.

Appendix A. The white-noise paraxial regime and the scintillation regime In this paper we consider a primary scaling regime in which the solutions of the Helmholtz equation (2.4) can be approximated in terms of the Green's function solving the Itô–Schrödinger equation (2.6). This is the white-noise paraxial regime where the propagation distance is large compared to the correlation length of the medium which is on the same scale as the beam radius (or source width), which in turn is large compared to the wavelength. The Itô–Schrödinger description allows us to get explicit expressions for the second-order moments of the wave field at a fixed frequency. In this paper we use the second moment at two frequencies to describe the mean refocused wave field in time reversal when we average with respect to the random medium in (2.2) corresponding to averaging with respect to the driving Brownian motion B in (2.6). It is also important to describe the statistical stability of empirical covariances or time-reversed fields when formed from one realization of the medium. Such statistical stability or SNR analysis requires expressions for the fourth moment of the wave field with the wave field components in the moment evaluated at different frequencies. In this paper we consider a secondary scaling regime, the scintillation regime, which allows us to get explicit expressions for the multifrequency moments of the wave field. The scintillation regime is valid in the paraxial white-noise regime when, additionally, the correlation length of the medium is small compared to the beam radius as described in section 5.3.

In this appendix we discuss these two scaling regimes, the paraxial white-noise and scintillation regimes, and the relation to the Itô–Schrödinger equation, and we refer to [13, 15] for the full derivation. Consider $\hat{u}(z, \boldsymbol{x})$ satisfying the Helmholtz equation (2.4). Let σ be the standard deviation of the fluctuations of the index of refraction n in this equation. Moreover, assume here that the random fluctuations of the index of refraction is isotropic and denote by $l_{\rm c}$ the correlation length of the fluctuations, by λ the wavelength, by L the typical propagation distance, and by r_o the transverse radius of the initial beam, which in this paper corresponds to the dimension of the time-reversal mirror. We introduce the wavenumber defined by

$$k = \frac{\omega}{c_o} = \frac{2\pi}{\lambda}, \tag{A.1}$$

with c_o the background wave speed. In this framework the variance $C(\mathbf{0})$ of the Brownian field in the Itô–Schrödinger equation (2.6) is of order $\sigma^2 l_{\rm c}$ and the transverse scale of variation of the covariance function $C(\boldsymbol{x})$ in (2.8) is of order $l_{\rm c}$.

First, we consider the primary (paraxial white-noise) scaling that leads to the Itô–Schrödinger equation (A.2), which corresponds to zooming in on a high-frequency beam that propagates over a distance that is large relative to the correlation length of the medium, which is itself large relative to the wavelength; moreover, the medium fluctuations are small. Explicitly, we assume the primary scaling when

$$\frac{l_{\rm c}}{r_o} \sim 1\,, \qquad \frac{l_{\rm c}}{L} \sim \theta\,, \qquad \frac{l_{\rm c}}{\lambda} \sim \theta^{-1}\,, \qquad \sigma^2 \sim \theta^3\,,$$

where θ is a small dimensionless parameter. We introduce dimensionless coordinates by

$$\boldsymbol{x} = l_{\rm c}\boldsymbol{x}', \qquad z = Lz', \qquad k = \frac{k'}{l_{\rm c}\theta}, \qquad \nu(Lz', l_{\rm c}\boldsymbol{x}') = \theta^{3/2}\nu'\Big(\frac{z'}{\theta}, \boldsymbol{x}'\Big),$$

with ν being the relative fluctuations of the random medium (2.2). Then dropping "primes" we find that in dimensionless coordinates the Helmholtz equation reads

$$\left(\theta^2\partial_z^2 + \Delta_{\boldsymbol{x}}\right)\hat{u}^\theta + \frac{k^2}{\theta^2}\left(1 + \theta^{3/2}\nu\left(\frac{z}{\theta}, \boldsymbol{x}\right)\right)\hat{u}^\theta = 0.$$

We look for the behavior of the slowly varying envelope v^θ for propagation distances of order one in the dimensionless coordinates

$$\hat{u}^\theta(z, \boldsymbol{x}) = \exp\Big(i\frac{kz}{\theta^2}\Big)v^\theta(z, \boldsymbol{x})$$

that satisfies (by the chain rule)

$$\theta^2\partial_z^2 v^\theta + \left(2ik\partial_z v^\theta + \Delta_{\boldsymbol{x}} v^\theta + \frac{k^2}{\theta^{1/2}}\nu\Big(\frac{z}{\theta}, \boldsymbol{x}\Big)v^\theta\right) = 0.$$

Heuristically, when $\theta \ll 1$ the backscattering term $\theta^2\partial_z^2 v^\theta$ can be neglected, and we obtain a Schrödinger-type equation in which the potential fluctuates in z on the scale θ and is of amplitude $\theta^{-1/2}$. This diffusion approximation then gives the Itô–Schrödinger equation or white-noise limit driven by a Brownian field

$$2ikdv + \Delta_{\boldsymbol{x}} v\, dz + k^2 v \circ dB(z, \boldsymbol{x}) = 0, \tag{A.2}$$

or (2.6). This heuristic derivation can be made rigorous as shown in [13]. This equation is written in Stratonovich form as represented by the $\circ$ symbol. This reflects the fact that we arrive at this description as a scaling limit of a physical model where the fluctuating random field ν multiplying the wave field u has a finite correlation length in the z-direction. The Stratonovich stochastic integral can be interpreted in the simplest case as the limit when the integrand is evaluated at the midpoint of the interval of increment of the driving Brownian field and thus naturally appears in the diffusion limit when ν is replaced by a driving Brownian field. Note that the Itô interpretation of (A.2) has the form

$$dv = \frac{i}{2k}\Delta_{\boldsymbol{x}} v\, dz - \frac{k^2 C(\boldsymbol{0})}{8} v dz + \frac{ik}{2} v\, dB(z, \boldsymbol{x}). \tag{A.3}$$

In this representation the last term integrates to a zero-mean martingale term, and the added damping term is the Stratonovich corrector. We then have for the mean field $\bar{v} = \mathbb{E}[v]$:

$$\partial_z \bar{v} = \frac{i}{2k}\Delta_{\boldsymbol{x}}\bar{v} - \frac{k^2 C(\boldsymbol{0})}{8}\bar{v}. \tag{A.4}$$

Here the damping term reflects scattering and transfer of energy from the coherent part of the wave field to the incoherent part so that the mean field is exponentially damped. Indeed the reciprocal of the damping parameter was referred to as the scattering mean free path in (5.29) and characterizes the distance a coherent wave can travel before wave energy is scattered to the incoherent part.

The representation (A.3) gives closed equations for moments of all orders. We can easily solve explicitly the first-order moment in (A.4) and also the second-order moment equations at a single frequency. As mentioned, however, there is no explicit

solution for the fourth moment equations. We discuss now the secondary scaling limit that we refer to as the scintillation regime where we can solve explicitly for the fourth moment both in the single frequency case (and also in the multifrequency case up to a second-order lateral scattering function that can be explicitly characterized in the case of relatively strong scattering). In the scintillation regime the correlation length of the medium l_c is smaller than the initial beam radius r_o. Moreover, the medium fluctuations are weak, and the beam propagates deep into the medium. We then get the modified scaling picture

$$\frac{l_c}{r_o} \sim \varepsilon\,, \qquad \frac{l_c}{L} \sim \theta\varepsilon\,, \qquad \frac{l_c}{\lambda} \sim \theta^{-1}\,, \qquad \sigma^2 \sim \theta^3\varepsilon\,, \tag{A.5}$$

and we assume $\theta \ll \varepsilon \ll 1$. This means that the paraxial white-noise limit $\theta \to 0$ is taken first, and we find

$$2ikdv^\varepsilon + \Delta_{\boldsymbol{x}} v^\varepsilon\, dz + k^2 v^\varepsilon \circ dB^\varepsilon(z, \boldsymbol{x}) = 0,$$

where the radius r_o^ε of the initial condition is of order ε^{-1}, the variance $C^\varepsilon(\mathbf{0})$ of the Brownian field B^ε is of order ε, and the propagation distance L^ε is of order ε^{-1}. Then the limit $\varepsilon \to 0$ is applied, corresponding to the scintillation regime. In the regime (A.5) the effective strength $k^2 C^\varepsilon(\mathbf{0}) L^\varepsilon$ of the Brownian field is of order one since $\sigma^2 l_c L/\lambda^2 \sim 1$. Moreover, $L^\varepsilon \lambda/(r_o^\varepsilon)^2$ is of order ε. That is, the typical propagation distance is smaller than the Rayleigh length of the initial beam. Here the Rayleigh length corresponds to the distance when the transverse radius of the beam has roughly doubled by diffraction in the homogeneous medium case and it is given by r_o^2/λ. Indeed, it is seen in section 5 that the propagation distance at which relevant phenomena arise in the random case is of the order of $r_o l_c/\lambda$, which is smaller than the Rayleigh distance of the homogeneous medium r_o^2/λ.

REFERENCES

[1] L. C. Andrews and R. L. Philipps, *Laser Beam Propagation Through Random*, SPIE Press, Bellingham, 2005.

[2] J. Bertolotti, E. G. van Putten, C. Blum, A. Lagendijk, W. L. Vos, and A. P. Mosk, *Non-invasive imaging through opaque scattering layers*, Nature, 491 (2012), pp. 232–234.

[3] P. Blomgren, G. Papanicolaou, and H. Zhao, *Super-resolution in time-reversal acoustics*, J. Acoust. Soc. Am., 111 (2002), pp. 230–248.

[4] L. Borcea, *Interferometric imaging and time reversal in random media*, in Springer Encyclopedia of Applied and Computational Mathematics, Springer, New York, 2011.

[5] D. Dawson and G. Papanicolaou, *A random wave process*, Appl. Math. Optim., 12 (1984), pp. 97–114.

[6] A. Derode, A. Tourin, and M. Fink, *Random multiple scattering of ultrasound. II. Is time reversal a self-averaging process?*, Phys. Rev. E, 64 (2001), 036606.

[7] S. Feng, C. Kane, P. A. Lee, and A. D. Stone, *Correlations and fluctuations of coherent wave transmission through disordered media*, Phys. Rev. Lett., 61 (1988), pp. 834–837.

[8] M. Fink, D. Cassereau, A. Derode, C. Prada, P. Roux, M. Tanter, J. Thomas, and F. Wu, *Time-reversed acoustics*, Rep. Prog. Phys., 63 (2000), pp. 1933–1995.

[9] J.-P. Fouque, J. Garnier, G. Papanicolaou, and K. Sølna, *Wave Propagation and Time Reversal in Randomly Layered Media*, Springer, New York, 2007.

[10] J.-P. Fouque, G. Papanicolaou, and Y. Samuelides, *Forward and Markov approximation: The strong-intensity-fluctuations regime revisited*, Wave Random Media, 8 (1998), pp. 303–314.

[11] I. Freund, M. Rosenbluh, and S. Feng, *Memory effects in propagation of optical waves through disordered media*, Phys. Rev. Lett., 61 (1988), pp. 2328–2331.

[12] J. Garnier and G. Papanicolaou, *Passive Imaging with Ambient Noise*, Cambridge University Press, Cambridge, 2016.

[13] J. Garnier and K. Sølna, *Coupled paraxial wave equations in random media in the white-noise regime*, Ann. Appl. Probab., 19 (2009), pp. 318–346.
[14] J. Garnier and K. Sølna, *Scintillation in the white-noise paraxial regime*, Comm. Partial Differ. Equ., 39 (2014), pp. 626–650.
[15] J. Garnier and K. Sølna, *Fourth-moment analysis for beam propagation in the white-noise paraxial regime*, Arch. Rational Mech. Anal., 220 (2016), pp. 37–81.
[16] J. Garnier and K. Sølna, *Focusing waves through a randomly scattering medium in the white-noise paraxial regime*, SIAM J. Appl. Math., 77 (2017), pp. 500–519.
[17] J. Garnier and K. Sølna, *Imaging through a scattering medium by speckle intensity correlations*, Inverse Probl., 34 (2018), 094003.
[18] J. Garnier and K. Sølna, *Non-invasive imaging through random media*, SIAM J. Appl. Math., 78 (2018), pp. 3296–3315.
[19] J. W. Goodman, *Statistical Optics*, Wiley, New York, 2000.
[20] A. Ishimaru, *Wave Propagation and Scattering in Random Media*, Academic Press, San Diego, 1978.
[21] A. Ishimaru, S. Jaruwatanadilok, and Y. Kuga, *Time reversal effects in random scattering media on superresolution, shower curtain effects, and backscattering enhancement*, Radio Sci., 42 (2007), RS6S28.
[22] O. Katz, E. Small, and Y. Silberberg, *Looking around corners and through thin turbid layers in real time with scattered incoherent light*, Nat. Photon., 6 (2012), pp. 549–553.
[23] G. Lerosey, J. de Rosny, A. Tourin, and M. Fink, *Time reversal of electromagnetic waves*, Phys. Rev. Lett., 92 (2004), 193904.
[24] G. Lerosey, J. de Rosny, A. Tourin, and M. Fink, *Focusing beyond the diffraction limit with far-field time reversal*, Science, 315 (2007), pp. 1120–1122.
[25] A. P. Mosk, A. Lagendijk, G. Lerosey, and M. Fink, *Controlling waves in space and time for imaging and focusing in complex media*, Nat. Photon., 6 (2012), pp. 283–292.
[26] G. Papanicolaou, L. Ryzhik, and K. Sølna, *Statistical stability in time reversal*, SIAM J. Appl. Math., 64 (2004), pp. 1133–1155.
[27] S. M. Popoff, A. Goetschy, S. F. Liew, A. D. Stone, and H. Cao, *Coherent control of total transmission of light through disordered media*, Phys. Rev. Lett., 112 (2014), 133903.
[28] S. Popoff, G. Lerosey, M. Fink, A. C. Boccara, and S. Gigan, *Image transmission through an opaque material*, Nat. Commun., 1 (2010), pp. 1–5.
[29] S. Rotter and S. Gigan, *Light fields in complex media: Mesoscopic scattering meets wave control*, Rev. Mod. Phys., 89 (2017), 015005.
[30] J. W. Strohbehn, ed., *Laser Beam Propagation in the Atmosphere*, Springer, Berlin, 1978.
[31] F. Tappert, *The parabolic approximation method*, in Wave Propagation and Underwater Acoustics, J. B. Keller and J. S. Papadakis, eds., Springer, Berlin, 1977, pp. 224–287.
[32] B. J. Ucsinski, *Analytical solution of the fourth-moment equation and interpretation as a set of phase screens*, J. Opt. Soc. Am. A, 2 (1985), pp. 2077–2091.
[33] I. M. Vellekoop, A. Lagendijk, and A. P. Mosk, *Exploiting disorder for perfect focusing*, Nat. Photon., 4 (2010), pp. 320–322.
[34] I. M. Vellekoop and A. P. Mosk, *Focusing coherent light through opaque strongly scattering media*, Opt. Lett., 32 (2007), pp. 2309–2311.
[35] I. M. Vellekoop and A. P. Mosk, *Universal optimal transmission of light through disordered materials*, Phys. Rev. Lett., 101 (2008), 120601.